

Evaluating optimal U for 3d transition-metal oxides within the SCAN+ U frameworkOlivia Y. Long ¹, Gopalakrishnan Sai Gautam ², and Emily A. Carter ^{2,3,*}¹*Department of Physics, Princeton University, Princeton, New Jersey 08544, USA*²*Department of Mechanical and Aerospace Engineering, Princeton University, Princeton, New Jersey 08544-5263, USA*³*Office of the Chancellor and Department of Chemical and Biomolecular Engineering, Box 951405, University of California, Los Angeles, Los Angeles, California 90095-1405, USA*

(Received 4 January 2020; revised manuscript received 13 February 2020; accepted 2 March 2020; published 8 April 2020)

Redox-active 3d transition-metal oxides (TMOs) are crucial ingredients for multiple sustainable energy applications, including solar cells, batteries, catalysis, and solar thermochemical water splitting. However, any predictive modeling, such as that employing density functional theory, needs to describe accurately the energetics of redox reactions involving transition metals, if new candidate materials are to be identified in a reliable fashion. Recently, we demonstrated that the state-of-the-art, strongly constrained and appropriately normed (SCAN) exchange-correlation functional requires a Hubbard U correction (determined, e.g., from experimental oxidation enthalpies) to reproduce the ground-state structure, lattice parameters, magnetic moments, and electronic properties of Ce-, Mn-, and Fe-based oxides. In the present work, we extend our approach to identify optimal U values for other 3d TMOs, specifically Ti, V, Cr, Co, Ni, and Cu, within the SCAN+ U framework. We determine optimal U values of 2.5, 1.0, 3.0, and 2.5 eV for Ti, V, Co, and Ni oxides, respectively, while Cr and Cu oxides best reproduce redox thermodynamics without any U correction at all. While the U values required for Ti, V, Co, and Ni are lower than those needed within the generalized gradient approximation (GGA) + U or local density approximation (LDA) + U approaches, inclusion of U makes non-negligible improvements in ground-state property evaluations of these oxides. Here we also validate our optimal U values by performing a number of transferability checks for each 3d material. A SCAN+ U framework (with an appropriately determined U) therefore is needed to assess accurately the ground-state energies and qualitatively consistent electronic structures for (most) first-row TMOs.

DOI: [10.1103/PhysRevMaterials.4.045401](https://doi.org/10.1103/PhysRevMaterials.4.045401)

I. INTRODUCTION

3d transition-metal oxides (TMOs) have a variety of applications, such as catalysis [1–3], energy storage [4–6], photovoltaics [7–9], etc. One such important field of application is solar thermochemical water/CO₂ splitting [10–13], which involves using an (transition-metal-based) oxide substrate and a two-step cycle to split water and/or CO₂, eventually generating renewable fuels or fuel precursors. In all of these applications, the redox capability of the transition metal plays an important role in the suitability and performance of the specific material used. Hence, any theoretical framework that aims to design novel materials for such applications, such as those using density functional theory (DFT) [14,15], should describe accurately the redox thermodynamics and other related properties (e.g., structural stability, electronic and magnetic properties) of TMOs and analogous materials.

One of the major approximations involved in using DFT is the choice of electron exchange-correlation (XC) functional. Recently, Perdew and co-workers developed the strongly constrained and appropriately normed (SCAN) functional, which satisfies all 17 known constraints for a given XC functional [16,17]. Further work also showed that SCAN performs sig-

nificantly better than the Perdew-Burke-Ernzerhof (PBE) [18] version of the generalized gradient correction (GGA) XC functional in reproducing accurate formation enthalpies [19] and correct ground-state structures [20,21] of several main group compounds. Notably, SCAN does not underbind the O₂ molecule [22], a notorious drawback of GGA functionals [23–25]. However, SCAN still remains susceptible to self-interaction errors (SIEs) [26,27], especially in 3d and 4f metals, which contain highly localized d and f orbitals, respectively. Such SIEs manifest in all sorts of erroneous predictions, including for oxidation enthalpies, ground-state structures, magnetic properties, and electronic structures [22]. Importantly, previous work has shown that the SIEs can be corrected using an “optimal” Hubbard U energy correction [28], resulting in a SCAN+ U framework [22] analogous to the GGA+ U theory that has been widely used to model TMOs [23,29]. Given that the actual U correction for each 3d metal is not known *a priori*, U either can be determined theoretically, e.g., using electrostatically embedded Hartree-Fock calculations (which are expensive) [30,31] or linear response theory [29,32–34] (which typically overestimates U due to DFT’s SIE and is unsuitable for closed shell ions [35]), or can be determined using experimental data, such as redox thermodynamics [23,36,37] or band gaps [38]. Indeed, the authors in Ref. [22] obtained U values for use with the SCAN functional that minimized errors in theoretical versus

*eac@ucla.edu

experimental oxidation enthalpies for various binary oxidation reactions of Mn, Fe, and Ce oxides.

In this work, we build on the framework developed by Gautam and Carter [22] to evaluate optimal U values across all $3d$ transition metals within the SCAN+ U framework, based on experimental oxidation enthalpies. Specifically, we consider the binary oxidation reactions for Ti, V, Cr, Co, Ni, and Cu oxides and obtain optimal U values of 2.5, 1.0, 0.0, 3.0, 2.5, and 0.0 eV, respectively. For each $3d$ oxide, beyond redox thermodynamics we evaluate their ground-state structural, magnetic, and electronic properties at various U values within SCAN+ U , and highlight key differences in the DFT-SCAN and SCAN+ U predictions for select systems. Additionally, for each $3d$ metal, we check for transferability of the obtained optimal U value by validating predictions made with SCAN + (optimal) U calculations with available experimental data on oxides not used in obtaining the optimal U . Specifically, we evaluated properties of (i) Ti_3O_5 (for Ti), (ii) V_3O_5 , V_4O_7 , and V_6O_{13} (for V), (iii) CrO and Cr_3O_4 (for Cr), (iv) SrCoO_3 and CoO_2 (for Co), (v) LiNiO_2 and NiCr_2O_4 (for Ni), and (vi) Cu_4O_3 (for Cu). Finally, we identify possible means to improve property predictions for $3d$ -based oxides using either DFT-SCAN or SCAN+ U .

II. METHODS

A. Computational methods

We utilized the Vienna *ab initio* simulation package (VASP) [39,40] to perform DFT calculations within the all-electron, frozen-core, projector-augmented-wave (PAW) formalism [41]. The specific PAW potentials used to describe the interaction of self-consistently optimized valence electrons with the nuclei and frozen-core electrons are listed in Table S1 of the Supplemental Material (SM) [42]. Since SCAN-derived PAW potentials are not yet available for several elements, we used PAW potentials derived at the PBE level in our work. We used a plane wave basis kinetic energy cutoff of 520 eV and a dense, Γ -point-centered, Monkhorst-Pack [43] k -point mesh (spacing $\leq 0.025 \text{ \AA}^{-1}$) to sample the Brillouin zone, consistent with Ref. [22]. Additionally, we used Gaussian smearing [44] to integrate over the Fermi surface, with a smearing width of 0.05 eV. Both DFT-SCAN and SCAN+ U were used to treat all the oxides (except Sc_2O_3 and ZnO , for which only DFT-SCAN was used; see SM), where the U was input to the rotationally invariant framework of Dudarev *et al.* [45]. We relaxed the lattice vectors, volume, and ionic positions of all the oxides for each U value, with the relaxation terminated once the total energies and atomic forces converged to $< 0.01 \text{ meV}$ and $< |0.03| \text{ eV/\AA}$, respectively.

B. Reaction energies

To determine the optimal U values for each TMO, we use the oxidation enthalpies of Ti, V, Cr, Co, Ni, and Cu oxides as our metric, similar to the framework in Ref. [22]. Schematically, the oxidation reaction among the above oxides can be written as $\text{MO}_x + \frac{z-x}{2}\text{O}_2 \rightarrow \text{MO}_z$. An exception is Ni oxides, where we considered the oxidation reaction $4\text{NiO} + 2\text{Li}_2\text{O} + \text{O}_2 \rightarrow 4\text{LiNiO}_2$, due to lack of reliable structural and thermodynamic data for Ni_2O_3 and NiO_2 , which are

the other possible binary Ni oxides. Standard formation enthalpies (i.e., at 298 K and 1 atm) for the various oxides from the Kubaschewski [46], Wagman [47], and Barin tables [48] are used to calculate the experimental oxidation enthalpy for the $\text{MO}_x \rightarrow \text{MO}_z$ reaction per mole of O_2 . The experimental values then are compared with the values calculated using DFT-SCAN and SCAN+ U for each oxidation reaction. The U values considered range from 0–6 eV, where $U = 0$ indicates a pure DFT-SCAN calculation. The ideal U value is determined by minimizing the absolute error between the theoretical and experimental reaction enthalpy for a given reaction. Subsequently, the optimal U value for a given $3d$ oxide system is obtained by averaging the ideal U values across possible oxidation reactions within the system. Thus, for a $3d$ metal with multiple possible oxidation reactions, the optimal U can be thought of as an averaged value that can be used across the various oxidation states of the $3d$ metal. Particularly for modeling systems where a given $3d$ metal can exhibit multiple oxidation states and/or the oxidation state is not known *a priori*, the optimal U represents the “best compromise” value. Notably, the optimal U may yield a small (or large) error depending on how different the ideal U is from the optimal value. As detailed in Ref. [22], we ignore the pressure-volume ($P\Delta V$) and zero-point energy (ZPE) contributions while comparing theoretical enthalpies to experimental data.

C. Crystal structures and magnetic configurations

The crystal structures used to determine the optimal U value for each $3d$ TMO system are shown in Fig. 1 and the structures used for transferability checks are displayed in Fig. S1 of the SM. All initial structures were obtained from the Inorganic Crystal Structure Database (ICSD) [49] and we only considered structures that are “ordered,” i.e., structures where occupancies of all atomic sites equal an integer. The space group of each structure used is specified in Table I. We considered ferromagnetic (FM) and antiferromagnetic (AFM) configurations for all structures, with Fig. 1 illustrating the ground-state magnetic configurations for each structure for SCAN + (optimal) U (see below).

All rocksalt ($Fm\bar{3}m$) oxides (VO, CoO, and NiO) exist in a type-2 AFM magnetic ground state [50,51], which we modeled using either a $2 \times 2 \times 2$ (for VO) or a $1 \times 2 \times 1$ (for CoO and NiO) supercell of the primitive rocksalt structure. For CuO, the ground-state AFM configuration (below 220 K [52–54]) was modeled using a $2 \times 1 \times 2$ supercell of the $C2/c$ structure, in accordance with Ref. [55]. In the primitive spinel structure of Co_3O_4 (Fig. 1), the tetrahedral sites are occupied by high-spin (HS) Co^{2+} ions (blue/green polyhedra), while low-spin (LS) Co^{3+} ions occupy the octahedral sites (brown polyhedra), with the Co^{2+} ions exhibiting AFM coupling [56]. Both Ti_2O_3 and Cr_2O_3 are hexagonal, corundum-like oxides ($R\bar{3}cR$), exhibiting a $\uparrow\downarrow\uparrow\downarrow$ and $\uparrow\downarrow\uparrow\downarrow$ AFM coupling, respectively [57–59]. V_2O_3 and VO_2 exhibit a structural distortion away from their 298 K form at lower temperatures. Specifically, V_2O_3 distorts from a hexagonal ($R\bar{3}c$) oxide to a monoclinic form ($I2/a$; Fig. 1) due to its antiferromagnetism [60], while VO_2 exhibits a similar monoclinic ($P21/c$; Fig. 1) distortion away from its room-temperature rutile structure

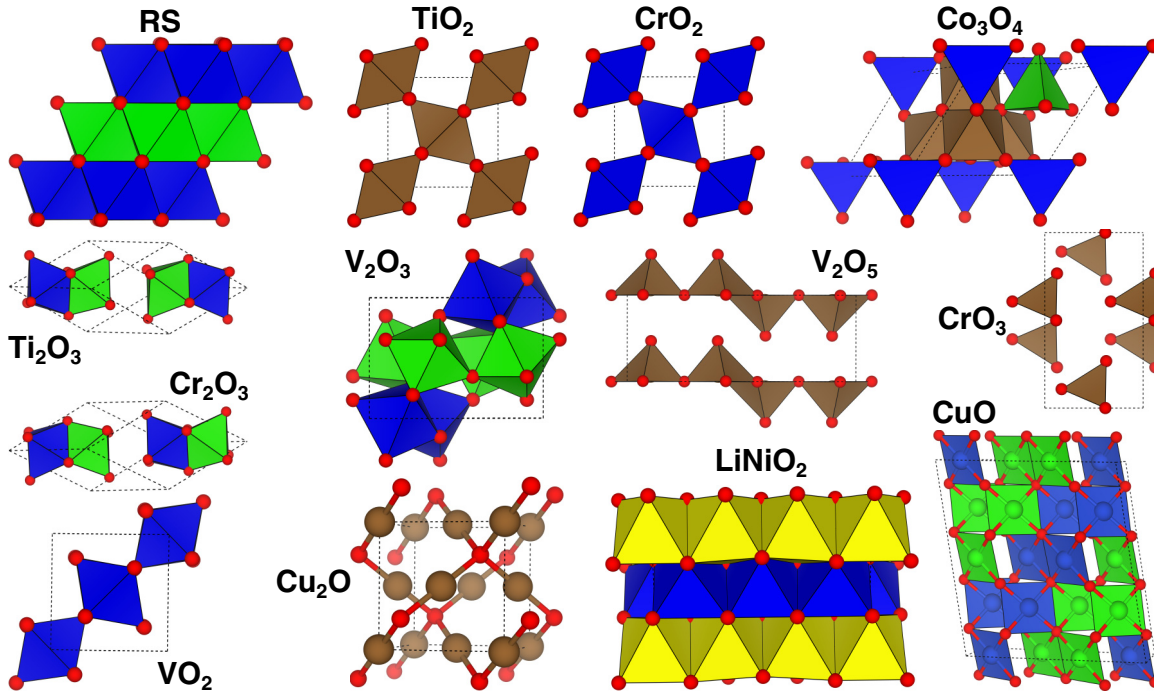


FIG. 1. Initial crystal structures considered in the oxidation reactions used to determine optimal U values. Blue, green, and brown polyhedra correspond to up spin, down spin, and no spin, respectively. Yellow polyhedra in LiNiO_2 indicate Li atoms. The magnetic configuration indicated for each oxide is its ground state at the SCAN + (optimal) U level.

($P42/mnm$) due to a metal-insulator transition (MIT) [61,62]. CrO_2 and TiO_2 exhibit rutile ground states at SCAN + (optimal) U (Fig. 1), while CrO_3 and V_2O_5 are known to crystallize in orthorhombic structures [63,64].

III. RESULTS

A. Oxidation energetics of transition-metal oxides

Figure 2 plots the oxidation reaction enthalpies (solid lines) as a function of applied U within SCAN+ U for Ti [panel (a)], V (b), Cr (c), Co (d), Ni (e), and Cu (f). For systems with multiple possible oxidation reactions [V and Cr; panels (b) and (c) in Fig. 2], individual reactions are distinguished by different colors. For example, all quantities corresponding to the $\text{V}_2\text{O}_3 \rightarrow \text{VO}_2$ oxidation in Fig. 2(b) are indicated with red symbols and lines. Horizontal dashed lines in each panel correspond to experimental oxidation enthalpies [46–48], with different colors distinguishing individual reactions. For example, the black dashed line in Fig. 2(c) highlights the oxidation enthalpy for the $\text{Cr}_2\text{O}_3 \rightarrow \text{CrO}_2$ reaction. Vertical dotted lines of a given color reflect the U value (i.e., ideal U) that minimizes the error between SCAN+ U oxidation enthalpy and experimental data for a given reaction. Additionally, dotted blue lines in all panels of Fig. 2 signify optimal U values for a given $3d$ metal, which is obtained by averaging the ideal U across individual oxidation reactions. For example, an optimal $U = 1.0$ eV for V is obtained by averaging the three ideal U values (0.2, 0.5, and 2.2 eV) across the possible oxidation reactions. Note that for systems with a single oxidation reaction considered [Ti, Co, and Ni; panels (a), (d), and (e) in Fig. 2], the optimal and ideal U values are identical. From here on, we use U_M to denote the optimal U value for the M $3d$ system.

To obtain optimal U values, we considered the oxidation of (i) $\text{Ti}_2\text{O}_3 \rightarrow \text{TiO}_2$ (+3 \rightarrow +4) in Ti [Fig. 2(a)], (ii) $\text{VO} \rightarrow \text{V}_2\text{O}_3$ (+2 \rightarrow +3), $\text{V}_2\text{O}_3 \rightarrow \text{VO}_2$ (+3 \rightarrow +4), and $\text{VO}_2 \rightarrow \text{V}_2\text{O}_5$ (+4 \rightarrow +5) in V [Fig. 2(b)], (iii) $\text{Cr}_2\text{O}_3 \rightarrow \text{CrO}_2$ (+3 \rightarrow +4) and $\text{CrO}_2 \rightarrow \text{CrO}_3$ (+4 \rightarrow +6) in Cr [Fig. 2(c)], (iv) $\text{CoO} \rightarrow \text{Co}_3\text{O}_4$ (+2 \rightarrow +2.67) in Co [Fig. 2(d)], (v) $\text{NiO} \rightarrow \text{LiNiO}_2$ (+2 \rightarrow +3) in Ni [Fig. 2(e)], and (vi) $\text{Cu}_2\text{O} \rightarrow \text{CuO}$ (+1 \rightarrow +2) in Cu [Fig. 2(f)]. Calculated properties of all oxides in Fig. 2 are tabulated in Table I while predicted oxidation states and electronic configurations of the $3d$ metal in each oxide are tabulated in Table III (see following sections). The choice of oxides used in Fig. 2 for each $3d$ system is motivated primarily by their thermodynamic stability and availability of reliable experimental data, including ground-state structures and formation enthalpies. For example, we do not consider the formation enthalpy of CrO and Cr_3O_4 when obtaining an optimal U value for Cr, even though experimental data are available for both oxides [65], because of their metastability. On the other hand, we had to consider the $\text{NiO} \rightarrow \text{LiNiO}_2$ oxidation for Ni because no reliable thermodynamic and/or structural data exist for Ni_2O_3 and NiO_2 , which constitute the other (possible) binary Ni oxides. Also, the specific choice of LiNiO_2 among several possible ternary Ni oxides was primarily because of the accurate thermodynamic description of binary Li oxides by DFT-SCAN [22].

For Ti, Co, and Ni oxides [panels (a), (d), and (e) in Fig. 2], we find that DFT-SCAN greatly overestimates (i.e., it is too negative) the oxidation enthalpies by ~ 0.8 , ~ 4 , and ~ 1.6 eV, respectively; adding a correction of $U_{\text{Ti}} = 2.5$ eV, $U_{\text{Co}} = 3.0$ eV, and $U_{\text{Ni}} = 2.5$ eV minimizes the errors between calculated and experimental values. The added U in these oxides thus makes a non-negligible improvement in the description

TABLE I. Experimental, DFT-SCAN, and SCAN+ U lattice constants (Å), lattice vector angles (deg), band gaps (eV), and magnetic moments M (μ_B , on the $3d$ ion) of all the transition-metal oxides considered in this work. Specific U values used are $U_{Ti} = 2.5$, $U_V = 1.0$, $U_{Co} = 3.0$, and $U_{Ni} = 2.5$ eV. SCAN+ U properties with applied U of 0.5 and 2.0 eV for Cr and Cu, respectively, are also given. The space group of the polymorph is given for each composition.

Composition (space group)	Source	Lattice constants (Å)			Lattice vector angles (deg)			Band gap (eV)	M (μ_B)
		a	b	c	α	β	γ		
Ti ₂ O ₃ ($R\bar{3}cR$)	Expt.	5.43	5.43	5.43	56.7	56.7	56.7	0.20 [69]	± 0.03 –0.20 [59,70]
	DFT-SCAN	5.45	5.45	5.45	55.8	55.8	55.8	Metallic	0.0
	SCAN+ U_{Ti}	5.58	5.58	5.54	56.3	56.1	55.9	1.11	± 0.86
TiO ₂ ($P4_2/mnm$)	Expt.	4.59	4.59	2.96	90.0	90.0	90.0	3.00 [71]	0 ^a
	DFT-SCAN	4.59	4.59	2.96	90.0	90.0	90.0	1.74	0 ^a
	SCAN+ U_{Ti}	4.62	4.62	2.99	90.0	90.0	90.0	2.06	0 ^a
VO ($Fm\bar{3}m$)	Expt.	5.83	5.83	5.83	60.0	60.0	60.0	N/A	N/A
	DFT-SCAN	6.31	6.31	5.83	57.2	57.2	60.0	0.41	± 2.43
	SCAN+ U_V	6.30	6.30	5.94	58.0	58.0	60.0	1.18	± 2.55
V ₂ O ₃ ($I2/a$)	Expt.	7.26	5.00	5.55	90.0	96.8	90.0	~ 0.2 [72]	1.20–2.37 [73,74]
	DFT-SCAN	7.24	5.01	5.56	90.0	97.1	90.0	Metallic	± 1.71
	SCAN+ U_V	7.27	5.10	5.56	90.0	96.5	90.0	0.36	± 1.80
VO ₂ ($P21/c$)	Expt.	5.75	4.54	5.38	90.0	122.6	90.0	0.70 [72]	~ 1 [75]
	DFT-SCAN	5.67	4.54	5.35	90.0	122.0	90.0	Metallic	1.09
	SCAN+ U_V	5.75	4.54	5.37	90.2	122.4	90.0	Metallic	1.2, 1.1
V ₂ O ₅ ($Pmmm$)	Expt.	11.54	3.57	4.38	90.0	90.0	90.0	2.50 [76]	0 ^a
	DFT-SCAN	11.55	3.55	4.31	90.0	90.0	90.0	1.56	0 ^a
	SCAN+ U_V	11.57	3.56	4.26	90.0	90.0	90.0	1.65	0 ^a
Cr ₂ O ₃ ($R\bar{3}cR$)	Expt.	5.36	5.36	5.36	55.1	55.1	55.1	3.20 [77]	± 2.76 [78]
	DFT-SCAN	5.36	5.36	5.36	55.0	55.0	55.0	1.18	± 2.73
	SCAN+ U	5.37	5.37	5.37	55.1	55.1	55.1	2.04	± 2.76
CrO ₂ ($P4_2/mnm$)	Expt.	4.42	4.42	2.92	90.0	90.0	90.0	Metallic [79]	2.0 [79]
	DFT-SCAN	4.41	4.41	2.91	90.0	90.0	90.0	Metallic	2.28
	SCAN+ U	4.41	4.41	2.92	90.0	90.0	90.0	Metallic	2.32
CrO ₃ ($C2cm$)	Expt.	4.79	8.56	5.74	90.0	90.0	90.0	3.80 [80]	0 ^a
	DFT-SCAN	4.70	8.53	5.70	90.0	90.0	90.0	1.86	0 ^a
	SCAN+ U	4.72	8.56	5.70	90.0	90.0	90.0	1.92	0 ^a
CoO ($Fm\bar{3}m$)	Expt.	3.01	6.01	3.01	60.0	60.0	60.0	2.40 [81,82]	± 3.35 –3.80 [28,83]
	DFT-SCAN	3.00	6.00	3.00	60.0	60.0	60.0	Metallic	± 2.57
	SCAN+ U_{Co}	3.01	6.01	3.01	60.4	60.1	60.0	1.59	± 2.71
Co ₃ O ₄ ^b ($Fd\bar{3}m$)	Expt.	5.71	5.71	5.71	60.0	60.0	60.0	1.60 [81]	± 3.02 , 0.0 [56]
	DFT-SCAN	5.69	5.69	5.69	60.0	60.0	60.0	Metallic	± 2.54 , 0.0
	SCAN+ U_{Co}	5.71	5.71	5.71	60.0	60.0	60.0	2.26	± 2.71 , 0.0
NiO ($Fm\bar{3}m$)	Expt.	2.95	5.91	2.95	60.0	60.0	60.0	4.30 [84]	± 1.64 –1.90 [28,85]
	DFT-SCAN	2.94	5.87	2.94	60.0	60.0	60.0	0.25	± 1.57
	SCAN+ U_{Ni}	2.95	5.89	2.95	60.0	60.0	60.0	2.24	± 1.68
LiNiO ₂ ($P1m1$)	Expt.	5.01	5.01	5.02	80.4	70.6	60.0	N/A	~ 1 [86,87]
	DFT-SCAN	5.11	4.87	5.06	78.6	67.9	58.4	Metallic	0.86
	SCAN+ U_{Ni}	5.10	4.86	5.07	78.6	67.8	58.4	0.14	0.99
Cu ₂ O($Pn\bar{3}m$)	Expt.	4.27	4.27	4.27	90.0	90.0	90.0	2.17–2.4 [88,89]	0 ^a
	DFT-SCAN	4.23	4.23	4.23	90.0	90.0	90.0	0.35	0 ^a
	SCAN+ U	4.23	4.23	4.23	90.0	90.0	90.0	0.50	0 ^a
CuO ($C2/c$)	Expt.	9.37	3.42	10.26	90.0	99.5	90.0	1.40 [89]	0.68 [55]
	DFT-SCAN	8.73	3.75	10.26	90.0	96.1	90.0	Metallic	± 0.59
	SCAN+ U	9.18	3.47	10.25	90.0	98.8	90.0	1.52	± 0.67

^aTi, V, Cr, and Cu are in their +4, +5, +6, and +1 oxidation states in TiO₂, V₂O₅, CrO₃, and Cu₂O, respectively, resulting in $M = 0 \mu_B$.

^bListed magnetic moments are for Co²⁺ (nonzero) and low-spin Co³⁺ (0.0) ions within Co₃O₄.

of redox thermodynamics. In the case of V oxides [Fig. 2(b)], the ideal U required to minimize deviations from experimental oxidation enthalpies decreases with increasing oxidation state of the oxides involved in the reaction. For example, the ideal U decreases from 2.2 eV (VO \rightarrow V₂O₃) to 0.5 eV (V₂O₃ \rightarrow

VO₂) and eventually 0.2 eV (VO₂ \rightarrow V₂O₅), resulting in an optimal U of ~ 1.0 eV. The decreasing ideal U with increasing oxidation state in V is consistent with the lower number of exchange interactions among fewer d electrons as V oxidizes.

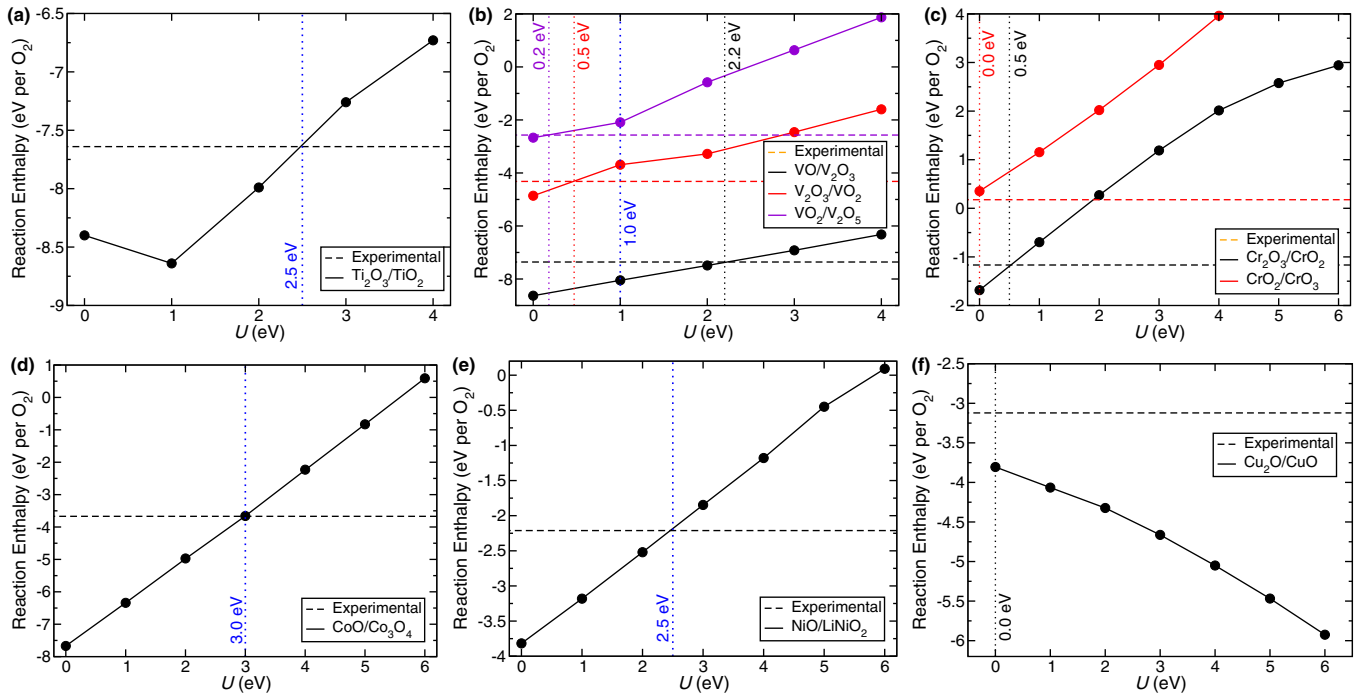


FIG. 2. Variation of the oxidation reaction enthalpy (solid lines) in (a) Ti, (b) V, (c) Cr, (d) Co, (e) Ni, and (f) Cu oxides with increasing magnitude of U within the SCAN+ U framework. Individual reactions are differentiated by colors for systems with multiple possible oxidations (e.g., V). Horizontal dashed line of a given color in each panel reflects the experimental oxidation enthalpy [46–48] for the reaction considered, with vertical dotted line of the same color signifying the U value that minimizes error between SCAN+ U predictions and experiments for the reaction. Blue dotted lines indicate optimal U , obtained by averaging the U values for individual oxidation reactions within a given system. Dashed yellow lines within the legends of panels (b) and (c) are simply placeholders, signifying that the horizontal dashed lines of a given color must be compared with solid and dotted (vertical) lines of the same color.

Similar to V, Cr oxides [Fig. 2(c)] also display a decreasing ideal U with increasing oxidation state, with $\text{Cr}_2\text{O}_3 \rightarrow \text{CrO}_2$ and $\text{CrO}_2 \rightarrow \text{CrO}_3$ requiring values of 0.5 and 0.0 eV, respectively. Surprisingly, exchange interactions in Cr oxides are better described than in V oxides by DFT-SCAN. For example, for an oxidation reaction involving the same number of d electrons ($3e^- \rightarrow 2e^-$), the U correction required for V (2.2 eV for $\text{VO} \rightarrow \text{V}_2\text{O}_3$) is higher compared to Cr (0.5 eV for $\text{Cr}_2\text{O}_3 \rightarrow \text{CrO}_2$), indicating lower exchange errors in Cr, despite the fact that one might expect the U correction would need to be larger for Cr than V due to the higher oxidation state contracting the d orbitals and therefore leading to larger exchange interactions. Interestingly, exchange errors in Cr are also lower than in Mn ($U_{\text{Mn}} = 2.7$ eV [22]), highlighting the anomalously good description of Cr oxides by DFT-SCAN. Note that previous studies [2,66,67] found negligible qualitative variations in total energy and band gap trends for differences of ± 0.5 eV in the magnitude of U used. Hence, given that the ideal U values for the two oxidation reactions of Cr oxides are 0.5 and 0.0 eV (yielding an average of 0.25 eV), we conclude that no U correction is required for describing Cr oxides with DFT-SCAN.

In the case of Cu [Fig. 2(f)], DFT-SCAN yields an oxidation enthalpy for $\text{Cu}_2\text{O} \rightarrow \text{CuO}$ of ~ -3.81 eV per O_2 , which overestimates the experimental enthalpy by ~ 0.7 eV. However, adding a U correction monotonically worsens the error between theoretical and experimental enthalpies, reaching an error of ~ 2.8 eV per O_2 at $U = 6$ eV. Thus, DFT-SCAN is

better than SCAN+ U in reproducing the redox behavior of Cu oxides, but with significant errors. Interestingly, Cu is the only $3d$ system that exhibits a decreasing (i.e., more negative) oxidation enthalpy with increasing U in SCAN+ U . Additionally, we found that including more outer-core electrons in the self-consistent description of Cu (i.e., including $3p$ states along with the valence $4s$ and $3d$ states self-consistently) detrimentally increases the deviation in oxidation enthalpy at both DFT-SCAN and SCAN+ U levels of theory, as indicated in Fig. S2 of the SM. Note that the PAW potentials used in this work are obtained at the PBE XC level because no libraries yet exist of SCAN-derived PAW potentials. Using PAW-PBE potentials therefore is another source of error [68], alongside the functional itself, in the DFT-SCAN (and SCAN+ U) oxidation enthalpies of Cu oxides, highlighting the challenges that remain in modeling Cu oxides with DFT-SCAN. Hereafter, unless specified otherwise, all results for Cu oxides using DFT-SCAN/SCAN+ U were calculated including the outer-core $3p$ states self-consistently.

B. Lattice parameters, band gaps, and magnetic moments

DFT-SCAN and SCAN+ U lattice constants, band gaps, and magnetic moments for all TMOs considered in Fig. 1 appear in Table I. The band gaps are obtained from corresponding density of states (DOS) calculations, which are provided for all oxides of Fig. 1 either as part of the following sections or in the SM (Figs. S3–S7). Particularly, Sec. S6

includes a detailed analysis on the calculated density of states for chromium oxides with DFT-SCAN and SCAN+ U . The calculated magnetic moment for a given oxide is averaged over all $3d$ ions within the structure that have the same type of spin (i.e., up/down). While Cr and Cu do not require a U correction with SCAN, we listed values corresponding to $U = 0.5$ and 2 eV for Cr and Cu systems, respectively, in Table 1 to highlight the sensitivity of the oxide properties to the addition of U . For Cr, we chose $U = 0.5$ eV since that is the ideal U for the $\text{Cr}_2\text{O}_3 \rightarrow \text{CrO}_2$ reaction, while the $\text{CrO}_2 \rightarrow \text{CrO}_3$ reaction does not require a U . Since the addition of U increases the error in redox properties of Cu oxides, we wanted to use a U that represents a “substantial” change from DFT-SCAN calculations yet is of physically “reasonable” magnitude. Specifically, the choice of U for Cu in SCAN+ U should be lower than the U typically used in GGA+ U calculations (~ 3.6 – 4 eV [23,90,91]), since the SCAN functional should exhibit lower SIE than GGA [16]. Also, the U for Cu should be lower than $U_{\text{Ni}} (= 2.5$ eV) in SCAN+ U since Cu’s oxidation states (+1/+2) are lower than Ni (+2/+3), which reflects a lower degree of contraction of Cu’s d states versus Ni’s d , and Cu’s d orbitals typically overlap better with O’s p orbitals than Ni [92], resulting in better delocalization of Cu’s d states and lower exchange interactions [93]. Hence, we used $U = 2$ eV for Cu oxides.

In general, SCAN+ U band gaps and magnetic moments (on the $3d$ ions) are in better qualitative agreement with experiments than those from DFT-SCAN across all $3d$ systems considered. DFT-SCAN typically underestimates band gaps compared to experiments, which is unsurprising as this theoretical framework (DFT) is only meant to capture ground-state electronic structure and is not supposed to reproduce the fundamental gap of a material [94]. DFT-SCAN and SCAN+ U both incorrectly predict metallic behavior in VO_2 , which usually undergoes a MIT at lower temperatures and is known to exhibit a band gap in its ground state [61,75]. By contrast, the addition of U leads to overestimations of band gaps compared to experiments in Ti_2O_3 (by ~ 0.9 eV), V_2O_3 (by ~ 0.16 eV), Co_3O_4 (by ~ 0.7 eV), and CuO (by ~ 0.12 eV) whereas DFT-SCAN wrongly predicts metallic behavior in these systems. The overestimation of band gaps by SCAN+ U in these oxides may be due to either a higher-than-required U (for band gap predictions specifically) and/or errors in interpretation of measurements (e.g., unintended doping during sample preparation). While band gap overestimation from DFT-SCAN, which is based on eigenvalue gaps rather than optical or quasiparticle (photoemission/inverse photoemission) gaps, is a definite indication of electronic structure prediction failure, SCAN+ U may overestimate band gaps depending on the U value used. The DFT-SCAN eigenvalue gap always should be smaller than the optical or quasiparticle gap because of the lack of the derivative discontinuity in the DFT exchange-correlation potential [26]. Adding an “appropriate” U correction can enable DFT to accurately reproduce the fundamental gap since the U correction restores (some of) the derivative discontinuity missing in pure DFT XC’s. However, DFT+ U may predict band gaps higher than experimental ones, particularly at large values of U .

As with band gap trends, both DFT-SCAN and SCAN+ U underestimate magnetic moments (versus experiments) on the

$3d$ ion in the oxides considered. Exceptions include Ti_2O_3 and CuO , where SCAN+ U overestimates the moments compared to experiments, and VO_2 and CrO_2 , where both DFT-SCAN and SCAN+ U overestimate. In the case of lattice parameters, both DFT-SCAN and SCAN+ U values deviate less than 3% from experiments for all structures except VO and CuO, highlighting reasonable agreement overall. In the case of VO, both DFT-SCAN and SCAN+ U exhibit $\sim 8\%$ error versus experiments while the error with DFT-SCAN is $\sim 9.6\%$ in CuO. Notably, a few oxides break their high-symmetry configurations during DFT-SCAN/SCAN+ U structure relaxations. For example, VO_2 , Ti_2O_3 , and CoO slightly deviate from their monoclinic, hexagonal, and rocksalt symmetries, respectively, in SCAN+ U , while VO breaks its rocksalt symmetry in both DFT-SCAN and SCAN+ U .

C. DFT-SCAN versus SCAN+ U in select systems

In this section, we highlight key predictive differences of DFT-SCAN and SCAN+ U for all oxides considered in Fig. 1, except for Cr oxides, which are discussed in Sec. S6 of the SM.

1. Polymorph selection in TiO_2

TiO_2 is known to exist in the rutile ($P42/mnm$; Fig. 1), anatase ($I4_1/amd$; Fig. S8 of SM), and brookite ($Pbca$; Fig. S8) polymorphs in nature, with rutile and anatase significantly more abundant than brookite [95]. Experimentally, rutile has been asserted to be the ground state of TiO_2 because the anatase \rightarrow rutile transition at $T > 873$ K is irreversible [95]. However, multiple quantum Monte Carlo (QMC) calculations yielded anatase as the ground state, with rutile stabilized at higher temperatures by vibrational entropy [96,97], with the observed irreversibility perhaps simply a kinetic trapping of rutile upon cooling. Interestingly, the QMC studies differ in the order of stability of brookite with respect to rutile. For example, Luo *et al.* [96] claim that the stability of TiO_2 decreases as anatase $>$ rutile $>$ brookite, in contrast to anatase $>$ brookite $>$ rutile found by Trail *et al.* [97]. Polymorph stabilities for TiO_2 are highly dependent on which XC functional is used within DFT, with the local density approximation (LDA) [15], LDA+ U , GGA, and/or GGA+ U yielding contrasting predictions [37,57,98–101].

Our calculations using DFT-SCAN and SCAN+ U_{Ti} also exhibit interesting trends, as highlighted in Fig. 3. We plot the relative energy (in meV/f.u.) of anatase (green triangles) and brookite (red squares) with respect to rutile, as a function of U in SCAN+ U . DFT-SCAN and SCAN+ U_{Ti} differ qualitatively in their predictions of the stable polymorph; namely, DFT-SCAN and SCAN+ U_{Ti} respectively predict anatase and rutile to be the ground state. Thus, DFT-SCAN agrees with QMC calculations while SCAN+ U agrees with current interpretations of experiments. Additionally, the order of stability with DFT-SCAN is anatase $>$ brookite $>$ rutile, while SCAN+ U_{Ti} predicts rutile $>$ brookite $>$ anatase. Given the wide-ranging discrepancies across theoretical and experimental studies for the ground-state structure of TiO_2 , future QMC calculations using DFT-SCAN/SCAN+ U_{Ti} geometries and wave functions as starting variables could prove definitive.

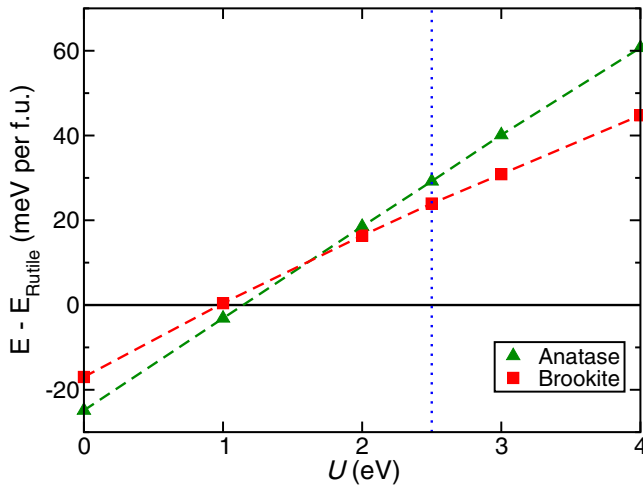


FIG. 3. Relative stability of anatase (green triangles) and brookite (red squares) TiO_2 , with respect to the rutile polymorph, plotted as a function of U in $\text{SCAN}+U$. The optimal U value for Ti ($U_{\text{Ti}} = 2.5$ eV) is indicated by the dotted blue line.

2. Electronic structure of V_2O_3

The calculated DOS in monoclinic ($I2/a$) V_2O_3 are shown in Fig. 4. Specifically, panels (a) and (b) display DOS at DFT-SCAN and $\text{SCAN}+U_V$ levels of theory, where $U_V = 1.0$ eV. Importantly, DFT-SCAN incorrectly predicts metallic behavior for V_2O_3 [Fig. 4(a)], despite the calculations already accounting for the hexagonal \rightarrow monoclinic distortion caused by the low-temperature antiferromagnetism of V_2O_3 [60,102]. Adding a U correction [Fig. 4(b)] improves qualitative agreement with the measured band gap (~ 0.2 eV [72]), despite $\text{SCAN}+U_V$ overestimating the gap (~ 0.36 eV). $\text{SCAN}+U_V$ also predicts Mott-Hubbard semiconducting behavior in V_2O_3 , signified by the predominant presence of V $3d$ states in both the VBM and the conduction band minimum (CBM), in agreement with experiments [72]. Thus, adding U to SCAN is important for improving the theoretical descrip-

tion of the electronic structure of binary V oxides and also will be relevant for multimetallic oxides containing V.

3. Polymorph selection in CoO

Experimentally, the ground state of CoO is known to be the rocksalt (RS; $Fm\bar{3}m$) structure with type-2 AFM (Fig. 1) at low temperatures [50]. However, CoO can also exist in the zinc blende (ZB; $F\bar{4}3m$) configuration [103], whose magnetic configuration is not known precisely. Note that the ZB structure can exhibit three different AFM configurations, types 1, 2 and 3 (see Fig. S9) [104], analogous to RS. Therefore, any theoretical framework used to model Co oxides should predict accurately both the ground-state structure and its precise magnetic configuration. Hence, we calculated the energies of ZB CoO in all three AFM configurations, alongside the FM configuration of RS, relative to AFM type-2 RS, and plotted it as a function of U (in $\text{SCAN}+U$) in Fig. 5(a). Notably, DFT-SCAN and $\text{SCAN}+U$ ($U = 1$ eV) incorrectly predict the AFM type-3 ZB configuration [green bars in Fig. 5(a)] as the ground state of CoO . Importantly, for $U = 2-6$ eV (including $U_{\text{Co}} = 3$ eV), $\text{SCAN}+U$ correctly predicts the AFM type-2 RS configuration to be the most stable.

Additionally, we evaluated the DOS for AFM type-2 RS [panels (b) and (c)] and AFM type-3 ZB [panels (d) and (e)] configurations CoO with DFT-SCAN [panels (b) and (d)] and $\text{SCAN}+U_{\text{Co}}$ [panels (c) and (e)], as displayed in Fig. 5. While DFT-SCAN incorrectly predicts the RS structure to be metallic, $\text{SCAN}+U_{\text{Co}}$ is in better qualitative agreement with experiments (band gap ~ 2.4 eV [81,82]) with a predicted band gap of ~ 1.59 eV. Analogous behavior can be observed with DFT-SCAN (metallic) and $\text{SCAN}+U_{\text{Co}}$ (band gap ~ 0.57 eV) calculations of the ZB CoO structure. Thus, the spurious stabilization of the ZB structure as the ground state of CoO by DFT-SCAN can be attributed to the incorrect electronic structure description of the RS structure by DFT-SCAN. Similarly, DOS calculations within spinel Co_3O_4 (see Fig. S6 of the SM) signify an incorrect metallic behavior prediction by DFT-SCAN while $\text{SCAN}+U_{\text{Co}}$ predicts a band

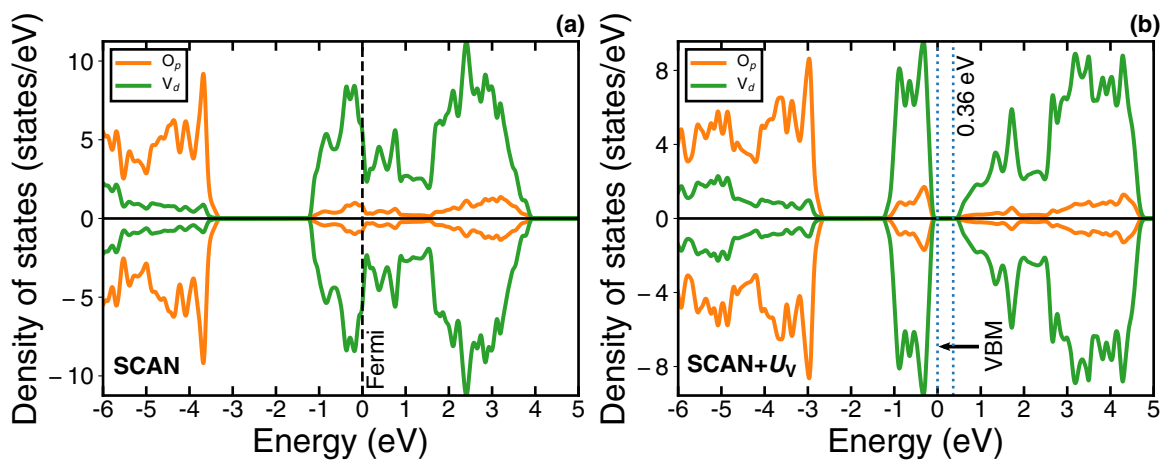


FIG. 4. DOS for V_2O_3 (space group: $I2/a$, AFM) calculated using DFT-SCAN [panel (a)] and $\text{SCAN}+U_V$ [$U_V = 1.0$ eV; panel (b)]. Orange and green curves respectively correspond to O $2p$ and V $3d$ states. Dashed black lines are Fermi levels in metallic system(s) while dotted blue lines are valence and conduction band edges for nonmetallic system(s). The zero on the energy scale is set to either the Fermi level (metals) or the valence band maximum (VBM, nonmetals). For structure(s) with a band gap, the value of the gap is indicated by the text annotation at the conduction band edge. States/eV plotted as negative are minority spin and states/eV above zero are majority spin.

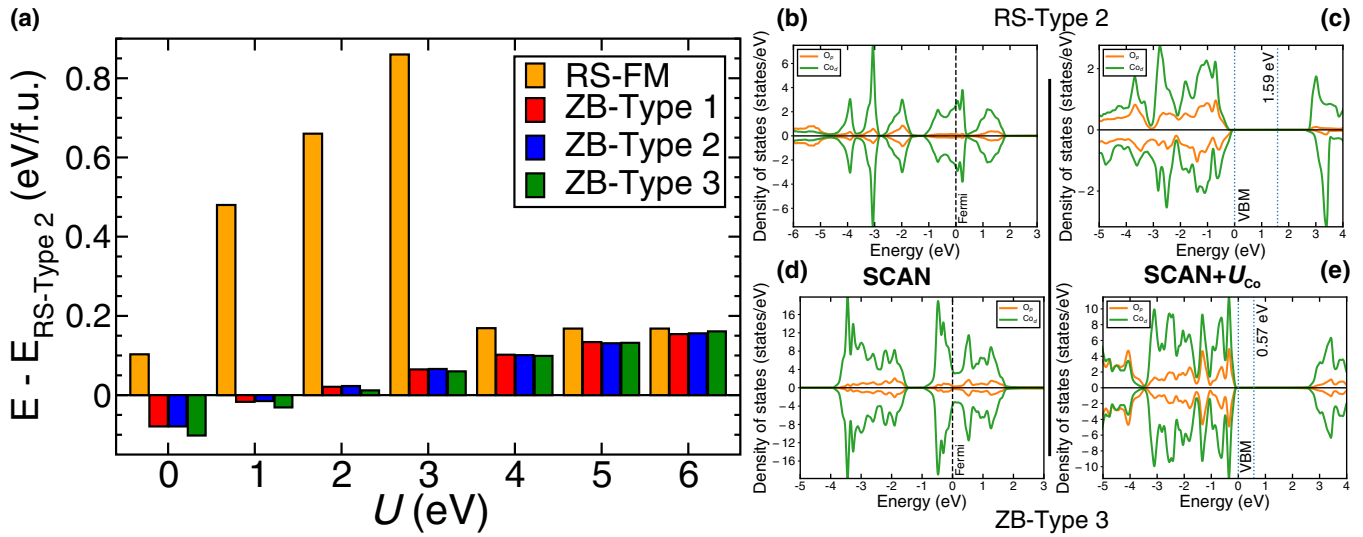


FIG. 5. Energies of different polymorphic and magnetic configurations of CoO [panel (a)], specifically, the FM configuration of rocksalt (RS) and AFM configurations (types 1, 2, and 3) of zinc blende (ZB), are plotted with respect to the energy of the type-2 AFM RS configuration. The relative energies predicted by SCAN+ U are plotted as a function of U value (0–6 eV). Panels (b) and (d) show the DOS predicted by DFT-SCAN while panels (c) and (e) display DOS from SCAN+ U , for type-2 AFM RS [panels (b) and (c)] and type-3 AFM ZB [panels (d) and (e)] CoO. Notations used within the DOS plots are identical to Fig. 4.

gap of ~ 2.26 eV, which compares better with experiments (band gap ~ 1.6 eV [81]). The apparent overestimation of Co_3O_4 's band gap by SCAN+ U_{Co} can be attributed largely to the measurement, which was obtained from a Li-doped sample [81]. Thus, the addition of U_{Co} (in SCAN+ U) is necessary to obtain the precise ground-state structure, magnetic configuration, and electronic properties in binary Co oxides.

4. Electronic structure of NiO

In its ground state, RS NiO exhibits an AFM type-2 configuration [50], and is known to be a wide-gap, charge-transfer insulator with a band gap of ~ 4.3 eV [84]. Figure 6 plots the DOS for the RS AFM type-2 configuration of NiO, as predicted by DFT-SCAN [panel (a)] and SCAN+ U_{Ni} [panel (b)], where $U_{\text{Ni}} = 2.5$ eV. Both frameworks correctly predict

the existence of a band gap, with SCAN+ U_{Ni} predicting a much wider gap (2.24 eV) than SCAN (0.25 eV), in better agreement with experiment. Moreover, SCAN+ U_{Ni} better captures the charge-transfer behavior observed experimentally, indicated by a similar number of Ni 3d and O 2p states at the VBM and predominantly Ni 3d states at the CBM [Fig. 6(b)]. By contrast, DFT-SCAN predicts both the VBM and CBM to be constituted predominantly by Ni 3d states [Fig. 6(a)]. Thus, the added U_{Ni} correction improves the electronic structure description of binary NiO.

5. Electronic structure of Cu oxides

To explore the effect of applying a U correction to the copper oxides, Cu_2O and CuO , we compare the DOS as predicted by DFT-SCAN [panels (a) and (b)] and SCAN+ U

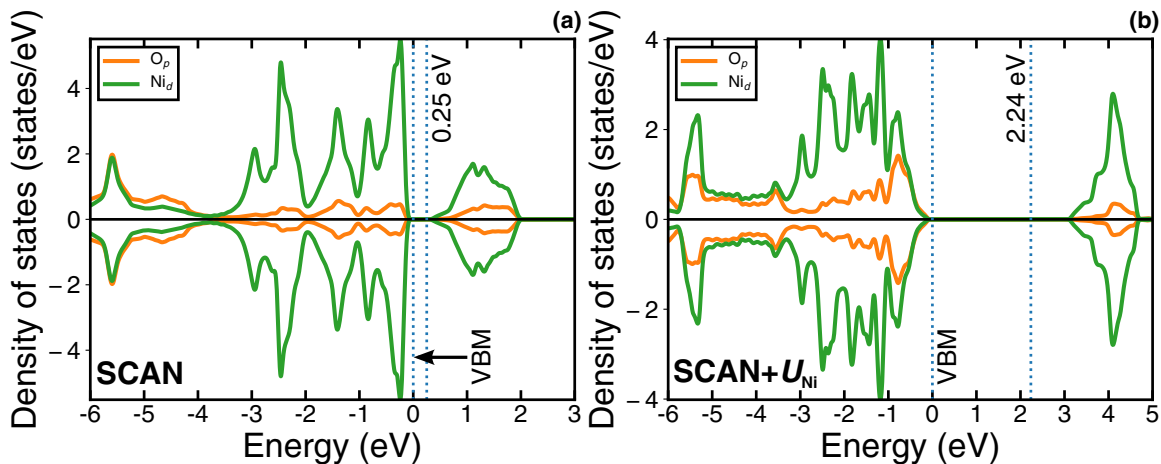


FIG. 6. DOS for the AFM type-2 configuration of rocksalt NiO, as calculated by (a) DFT-SCAN and (b) SCAN+ U_{Ni} ($U_{\text{Ni}} = 2.5$ eV). Notations used within each panel are identical to Fig. 4.

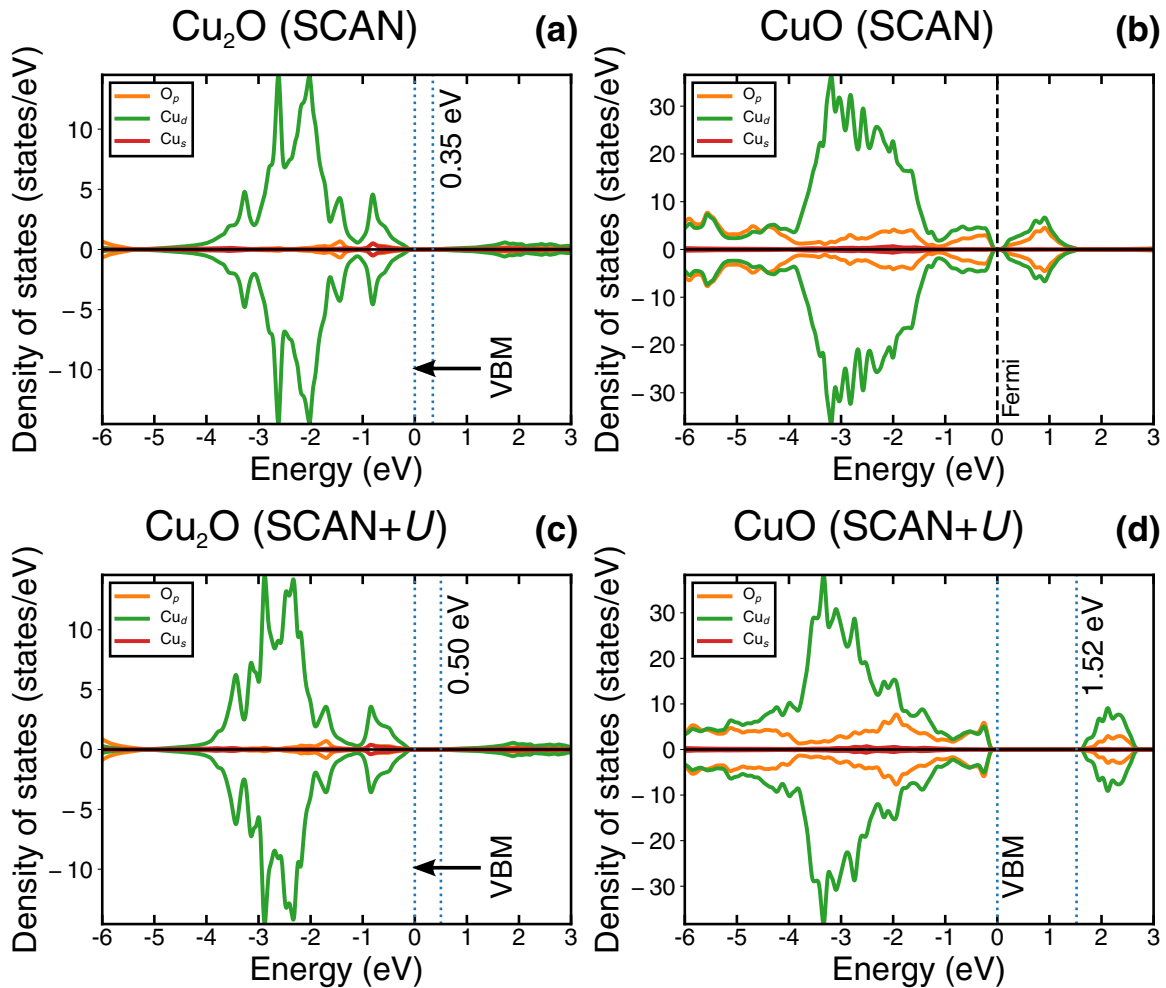


FIG. 7. DOS for [panels (a) and (c)] cubic Cu_2O and [panels (b) and (d)] AFM, monoclinic CuO , as calculated by DFT-SCAN (top row) and SCAN+ U (bottom row), where $U = 2$ eV. Orange, green, and red lines indicate states corresponding to O $2p$, Cu $3d$, and Cu $4s$ states, respectively. Notations used within each panel are identical to Fig. 4.

with $U = 2$ eV [panels (c) and (d)] in Fig. 7. We evaluated the DOS in the ground-state configurations of cubic, nonmagnetic Cu_2O (space group: $Pn\bar{3}m$) and AFM, monoclinic CuO (space group: $C2/c$). Notably, both Cu_2O and CuO are p -type semiconductors with band gaps of ~ 2.17 – 2.4 eV [88,89] and 1.4 eV [89], respectively. As in CrO_3 [Figs. S5(c) and S5(f)], DFT-SCAN and SCAN+ U both correctly predict a band gap in Cu_2O , with SCAN+ U giving a slightly better value of ~ 0.50 eV compared to ~ 0.35 eV produced by SCAN. On the other hand, DFT-SCAN and SCAN+ U yield significantly different electronic properties of CuO , analogous to CoO [Figs. 5(b) and 5(c)]. Specifically, DFT-SCAN incorrectly predicts metallic behavior in CuO , while SCAN+ U correctly produces a band gap, giving a marginally overestimated value of ~ 1.52 eV. Thus, although DFT-SCAN exhibits the lowest error in the oxidation enthalpy $\text{Cu}_2\text{O} \rightarrow \text{CuO}$ [Fig. 2(f)], applying a U correction may be necessary to model accurately the electronic structure of copper oxides.

D. Transferability of optimal U values

To test the transferability of the determined optimal U values, we implemented a number of checks for each TMO

using structures that were not used in obtaining the optimal U values (see Fig. S1 for an illustration of all structures used). The choice of specific oxides used in testing the U 's transferability was motivated primarily by the availability of experimental data (i.e., structural, thermodynamic, magnetic, and/or electronic). We also restricted our efforts, wherever possible, to binary $3d$ oxides, instead of ternary (and higher component) oxides to reduce secondary sources of error arising from poor description of the other component(s) present in the oxide. Beyond the results below, Sec. S11 of the SM contains supplemental data relevant to cobalt oxides, while transferability checks performed on nickel and copper oxides are included in Secs. S12 [105–107] and S13 [53,108,109].

1. Titanium oxides: Ti_3O_5

Beyond TiO_2 and Ti_2O_3 , Ti_3O_5 (monoclinic, $C2/m$; Fig. S1) is the only other binary Ti oxide with reliable experimental data for its structure [110] and formation enthalpy [46]. Note that Ti_3O_5 is a mixed oxide containing a 2:1 ratio of Ti^{3+} and Ti^{4+} ions. We calculated the enthalpy for Ti_3O_5 oxidizing to TiO_2 using both DFT-SCAN and SCAN+ U_{Ti}

TABLE II. Oxidation enthalpy of the $\text{Ti}_3\text{O}_5 \rightarrow \text{TiO}_2$ reaction, as calculated by DFT-SCAN and SCAN+ U_{Ti} ($U_{\text{Ti}} = 2.5$ eV), shown alongside the experimental value.

Reaction	Source	Reaction enthalpy (eV/O ₂)
$2\text{Ti}_3\text{O}_5 + \text{O}_2 \rightarrow 6\text{TiO}_2$	Expt.	-7.77
	DFT-SCAN	-8.50
	SCAN+ U_{Ti}	-8.08

($U_{\text{Ti}} = 2.5$ eV) and tabulated the values in Table II. Notably, the addition of U_{Ti} reduces the error in the $\text{Ti}_3\text{O}_5 \rightarrow \text{TiO}_2$ oxidation enthalpy, compared to experiment, from ~ 0.73 eV/O₂ with DFT-SCAN to ~ 0.31 eV/O₂ with SCAN+ U_{Ti} . Although SCAN+ U_{Ti} does not eliminate completely the error in oxidation enthalpy prediction, the significant reduction in the magnitude of the error highlights the importance of modeling all Ti oxides at the SCAN+ U_{Ti} level of theory.

2. Vanadium oxides: V_3O_5 , V_4O_7 , and V_6O_{13}

For V, we checked the transferability of U_{V} (1.0 eV), by considering the oxidation reactions of a few other binary V oxides, which were not used in Fig. 2(b). Specifically, we considered the oxidation reactions of $\text{V}_2\text{O}_3 \rightarrow \text{V}_3\text{O}_5$ (black circles and lines in Fig. 8), $\text{V}_2\text{O}_3 \rightarrow \text{V}_4\text{O}_7$ (red), and $\text{VO}_2 \rightarrow \text{V}_6\text{O}_{13}$ (purple) at different values of U with SCAN+ U . The choice of V_3O_5 , V_4O_7 , and V_6O_{13} was motivated primarily by the availability of reliable structures (Fig. S1) [49], the presence of mixed V oxidation states, and experimental thermodynamic data [47] (horizontal dashed lines in Fig. 8). We find that the ideal U (vertical dotted lines in Fig. 8) for these three oxidation reactions lies within a ± 0.5 eV range from $U_{\text{V}} =$

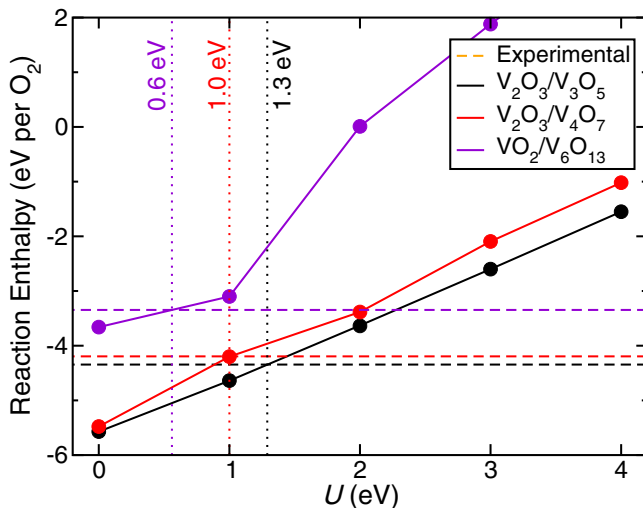


FIG. 8. Oxidation enthalpies of $\text{V}_2\text{O}_3 \rightarrow \text{V}_3\text{O}_5$ (black circles and lines), $\text{V}_2\text{O}_3 \rightarrow \text{V}_4\text{O}_7$ (red), and $\text{VO}_2 \rightarrow \text{V}_6\text{O}_{13}$ (purple), plotted with respect to U in SCAN+ U . Horizontal dashed lines and vertical dotted lines indicate experimental oxidation enthalpies and ideal U values, respectively, with the color of each line reflecting the corresponding oxidation reaction (e.g., black lines correspond to $\text{V}_2\text{O}_3 \rightarrow \text{V}_3\text{O}_5$).

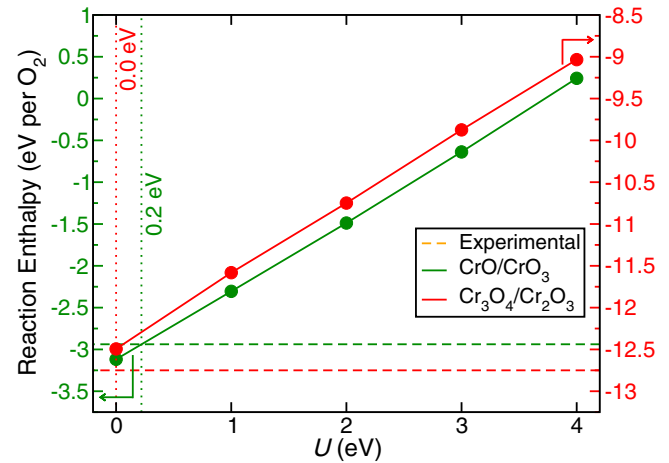


FIG. 9. Variation of the oxidation reaction enthalpy (solid lines) for the oxidation reactions $\text{CrO} \rightarrow \text{CrO}_3$ (green line and left vertical axis) and $\text{Cr}_3\text{O}_4 \rightarrow \text{Cr}_2\text{O}_3$ (red line and right vertical axis) with increasing magnitude of U within the SCAN+ U framework. The horizontal dashed lines display the experimental reaction enthalpies [47,65] while the vertical dotted lines mark the ideal U values for each reaction.

1.0 eV. For example, $\text{V}_2\text{O}_3 \rightarrow \text{V}_3\text{O}_5$, $\text{V}_2\text{O}_3 \rightarrow \text{V}_4\text{O}_7$, and $\text{VO}_2 \rightarrow \text{V}_6\text{O}_{13}$ require ideal U values of 1.3, 1.0, and 0.6 eV, respectively, to minimize deviations from experimental data. Similar to Fig. 2(b), the ideal U values decrease monotonically as the oxidation states of V involved in the oxidation reaction increase, reflecting the lower number of available d electrons (and hence lower SIE). Thus, $U_{\text{V}} = 1.0$ eV presents a reliable correction that can be used across various oxidation states of V.

3. Chromium oxides: CrO and Cr_3O_4

Figure 9 plots the predicted reaction enthalpies for the oxidation reactions $\text{CrO} \rightarrow \text{CrO}_3$ (green line and left vertical axis) and $\text{Cr}_3\text{O}_4 \rightarrow \text{Cr}_2\text{O}_3$ (red line and right vertical axis) as a function of the U used in SCAN+ U calculations. The horizontal dashed lines (green and red) correspond to the experimental reaction enthalpies [47,65], while the vertical dotted lines (green and red) mark the ideal U values for each reaction ($\text{CrO} \rightarrow \text{CrO}_3$ and $\text{Cr}_3\text{O}_4 \rightarrow \text{Cr}_2\text{O}_3$). We did not use CrO and Cr_3O_4 for obtaining our optimal U value [Fig. 2(c)] because both oxides are metastable [65].

While CrO is known to crystallize as RS, its precise magnetic configuration is unknown. Hence, we considered the three common types of AFM configurations in RS (types 1–3 [104]) along with the FM configuration; we found the AFM type-2 configuration (schematic in Fig. 1) to be the lowest-energy state for both DFT-SCAN and SCAN+ U . For spinel- Cr_3O_4 [111], we only considered the FM configuration as several different AFM configurations are possible within the spinel conventional cell; enumerating and calculating energies for all such configurations is beyond the scope of this work. The spinel- Cr_3O_4 structure is similar to spinel- Co_3O_4 shown in Fig. 1, with Cr^{2+} and Cr^{3+} ions occupying the tetrahedral and octahedral sites, respectively. Note that the oxidation reaction $\text{CrO} \rightarrow \text{CrO}_3$ represents the change across the +2

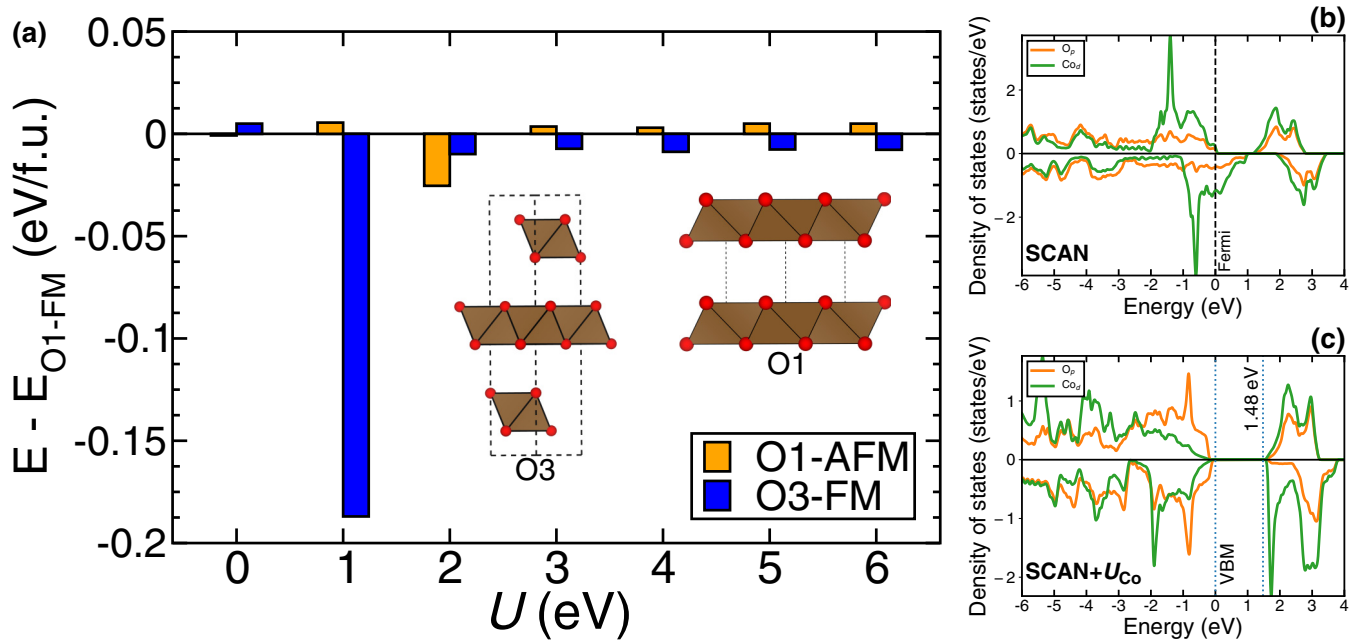


FIG. 10. Relative energies of AFM O1-CoO₂ and FM O3-CoO₂ with respect to the energy of FM O1-CoO₂ [panel (a)]. DOS of FM O1-CoO₂ predicted by DFT-SCAN (b) and SCAN+ U_{Co} (c), where $U_{\text{Co}} = 3.0$ eV. The inset figures in panel (a) show the rhombohedral, layered O3-CoO₂ (space group: $R\bar{3}mH$) and the hexagonal, layered O1-CoO₂ (space group: $P\bar{3}m1$) structures. Notations used in panels (b) and (c) are identical to Fig. 4.

to +6 oxidation states of Cr. Thus, the ideal U value found for this reaction (~ 0.2 eV; dotted green line in Fig. 9) can be interpreted as the average across ideal U values for all possible oxidation states of Cr. As the ideal U value for $\text{CrO} \rightarrow \text{CrO}_3$ is within the ± 0.5 eV range of tolerance [2,66,67] from $U = 0$ eV, we confirm that no U correction is needed for Cr oxides when using SCAN for XC. Similarly, the predicted oxidation enthalpies for the $\text{Cr}_3\text{O}_4 \rightarrow \text{Cr}_2\text{O}_3$ indicate that a U correction is not required with SCAN for Cr oxides (dotted red line in Fig. 9).

4. Cobalt oxides: SrCoO₃ and CoO₂

To validate the transferability of U_{Co} , we examined the cubic oxide perovskite, SrCoO₃, and the metastable binary layered oxide, CoO₂. We chose SrCoO₃ because it is one of the few compounds that has Co⁴⁺ in its intermediate spin (IS) configuration, corresponding to three unpaired d electrons, instead of the typical low spin (LS) configuration (one unpaired d electron). Experimentally, the magnitude of the magnetic moment on Co⁴⁺ in SrCoO₃ has been reported to be $\sim 2.5 \mu_{\text{B}}$ [112]. In both DFT-SCAN and SCAN+ U_{Co} calculations, we attempted initializing the Co⁴⁺ with different spin states, high spin (HS; five unpaired electrons), IS, and LS; the results are tabulated in Table S2 of the SM. Compared to DFT-SCAN, SCAN+ U_{Co} better predicts the magnetic moment on the Co⁴⁺ ions in SrCoO₃, giving $\sim 2.91 \mu_{\text{B}}/\text{Co}^{4+}$ as opposed to $\sim 2.05 \mu_{\text{B}}/\text{Co}^{4+}$ predicted by DFT-SCAN (Table S2). Notably, $\sim 2.91 \mu_{\text{B}}$ better represents three unpaired electrons on Co⁴⁺ compared to $\sim 2.05 \mu_{\text{B}}$, although the absolute error with respect to experiment is quite similar for both DFT-SCAN and SCAN+ U_{Co} . Also, applying the U_{Co} correction yields lattice parameters that agree better with experimental values (also

listed in Table S2), while both DFT-SCAN and SCAN+ U_{Co} correctly predict metallic behavior [112] (DOS plotted in Fig. S10). Thus, SCAN+ U_{Co} does model SrCoO₃ qualitatively better than DFT-SCAN.

Unlike the stable oxides CoO and Co₃O₄, CoO₂ is metastable with a hexagonal, layered [113] [O1 [114]; inset of Fig. 10(a)] structure. CoO₂ typically forms via de-lithiation of O3-LiCoO₂ [114], with the O1 structure known to be a Pauli paramagnetic metal experimentally, containing LS Co⁴⁺ ions ($\sim 0.15 \mu_{\text{B}}/\text{Co}^{4+}$) [115]. Figure 10(a) plots the energies of AFM O1-CoO₂ (orange bars) and FM O3-CoO₂ (blue bars), referenced to the energy of the FM O1-CoO₂ state, with the corresponding structures depicted in the insets of Fig. 10(a). Note that O3-CoO₂ is isostructural to O3-LiCoO₂, with the only difference being the absence of Li ions. For AFM O1-CoO₂, we considered an AFM coupling between adjacent Co⁴⁺ layers while all Co ions within a given layer are FM-coupled. Interestingly, DFT-SCAN correctly yields O1-CoO₂ as the ground state and correctly finds essentially no preference between FM and AFM (differing only by ~ 0.05 meV/f.u.), consistent with disordered magnetism characteristic of paramagnets. On the other hand, SCAN+ U_{Co} ($U_{\text{Co}} = 3.0$ eV) incorrectly predicts the O3-CoO₂ to be the stable polymorph by ~ 10 meV/f.u. Thus, DFT-SCAN appears to reproduce experimental magnetic and geometric structure marginally better than SCAN+ U_{Co} .

The DOS for FM O1-CoO₂, i.e., the experimental ground state, as predicted by DFT-SCAN and SCAN+ U_{Co} ($U_{\text{Co}} = 3.0$ eV), are plotted in Figs. 10(b) and 10(c), respectively (the DOS for AFM O1-CoO₂ are plotted in Fig. S6). Importantly, DFT-SCAN correctly predicts metallic behavior in O1-CoO₂, while SCAN+ U_{Co} predicts a large band gap (1.48 eV). Thus, the discrepancy between experiment and the SCAN+ U_{Co}

ground-state prediction is due to the incorrect electronic structure description. For O1-CoO₂, we also find that DFT-SCAN is better at reproducing the interlayer spacing, while SCAN+ U_{Co} further overshoots the experimental value (see Table S3 of the SM), highlighting again that DFT-SCAN models CoO₂ better than SCAN+ U_{Co} . One source of error in the predicted lattice parameters (and consequently, the electronic properties) is the lack of van der Waals dispersion corrections included in either DFT-SCAN or SCAN+ U_{Co} . Although DFT-SCAN appears to capture short and intermediate range dispersion corrections [16], the explicit addition of long-range dispersion interactions improves property predictions in layered compounds [21,116,117]. Hence, we plan to explore in future work the effects of adding van der Waals interactions with DFT-SCAN/SCAN+ U_{Co} in layered Co oxides. Finally, given the contrasting performance of SCAN+ U_{Co} in predicting the properties of SrCoO₃ and CoO₂, utilizing a U_{Co} correction with SCAN has to be done with care for Co-based oxides. Specifically, *a priori* knowledge of whether a given material/structure is metallic or not will enable determination of whether the SCAN+ U_{Co} framework predicts the correct electronic structure and whether SCAN+ U_{Co} can be trusted for any further property predictions.

IV. DISCUSSION

In this work, we obtained optimal U values within the SCAN+ U framework for six 3d TMO systems, including Ti, V, Cr, Co, Ni, and Cu, using experimental oxidation enthalpies as the metric to match. We found that optimal U corrections of 2.5, 1.0, 3.0, and 2.5 eV are required to describe reliably the redox thermodynamics, ground-state structure, electronic behavior, and magnetic properties of Ti, V, Co, and Ni oxides, respectively. In the case of Cr, DFT-SCAN is more accurate across all considered properties of binary Cr oxides whereas for Cu, DFT-SCAN (SCAN+ U) is better for redox thermodynamics (electronic behavior). Along with our previous work [22], we now have a library of optimal U corrections that can be used with SCAN across the 3d row (plus Ce), as summarized in Table III. Note that the U correction required with SCAN is consistently lower than typically used with GGA and/or LDA XC for the 3d systems considered here [23]. For example, U_{Ni} in GGA+ U obtained using oxidation enthalpies for Ni oxides is ~ 6.4 eV [23], ~ 4 eV higher than the optimal U reported here. SCAN thus incurs a lower SIE across all 3d systems compared to GGA and LDA functionals, further motivating the use of SCAN(+ U) for such systems. Additionally, we evaluated the transferability of the optimal U values by benchmarking properties calculated with DFT-SCAN and SCAN+ U for oxide systems not used in obtaining the optimal U . Specifically, we found robust transferability of all optimal U values except for U_{Co} , which predicts the wrong ground-state electronic and geometric structures for metastable CoO₂. Finally, we identified a few remaining challenges in accurately modeling 3d oxides using DFT-based techniques.

Along with the optimal U , Table III lists the specific oxides, the oxidation states, and the d electronic configuration on the 3d ion for each oxide used in obtaining the optimal U . Interestingly, the ideal U correction required to oxidize

TABLE III. Optimal U values for 3d transition metals and Ce within the SCAN+ U framework. Also listed are the oxidation states and the electronic spin configuration on the metal ion within each oxide used in obtaining an optimal U value.

Element	Oxidation state(s) used in fit	3d/4f configuration(s)					Optimal U value (eV)
Sc	+3 (Sc ₂ O ₃)						0.0 ^a
Ti	+3 (Ti ₂ O ₃)	↑					2.5
V	+4 (TiO ₂)						
	+2 (VO)	↑	↑	↑			
	+3 (V ₂ O ₃)	↑	↑				1.0
	+4 (VO ₂)	↑					
Cr	+5 (V ₂ O ₅)						
	+3 (Cr ₂ O ₃)	↑	↑	↑			
	+4 (CrO ₂)	↑	↑				0.0
Mn	+6 (CrO ₃)						
	+2 (MnO)	↑	↑	↑	↑	↑	
	+3 (Mn ₂ O ₃)	↑	↑	↑	↑	↑	2.7 [22]
Fe ^b	+4 (MnO ₂)	↑	↑	↑			
	+2 (FeO)	↑↓	↑	↑	↑	↑	3.1 [22]
Co	+3 (Fe ₂ O ₃)	↑	↑	↑	↑	↑	
	+2 (CoO)	↑↓	↑↓	↑	↑	↑	3.0
Ni	+2.66 (Co ₃ O ₄) ^c	↑↓	↑↓	↑↓			
	+2 (NiO)	↑↓	↑↓	↑↓	↑	↑	2.5
Cu	+3 (LiNiO ₂)	↑↓	↑↓	↑↓	↑		
	+1 (Cu ₂ O)	↑↓	↑↓	↑↓	↑↓	↑↓	0.0
Zn	+2 (CuO)	↑↓	↑↓	↑↓	↑↓	↑	
	+2 (ZnO)	↑↓	↑↓	↑↓	↑↓	↑↓	0.0 ^a
Ce	+4 (CeO ₂)						2.0 [22]
	+3 (Ce ₂ O ₃)	↑					

^aNo redox activity typical in the solid state.

^bSpin configuration of Fe not shown in Fe₃O₄.

^cSpin configuration indicated is Co³⁺ within Co₃O₄.

the “first” d electron (in the least oxidized, stable TMO) is similar (i.e., between 2.2–3.1 eV) across the entire 3d series (with the notable exception of Cr). For example, the ideal U values going from $d^1 \rightarrow d^0$, $d^3 \rightarrow d^2$, $d^5 \rightarrow d^4$, $d^6 \rightarrow d^5$, $d^7 \rightarrow d^6$, and $d^8 \rightarrow d^7$ in Ti (2.5 eV), V (2.2 eV), Mn (2.9 eV [22]), Fe (2.9 eV [22]), Co (3.0 eV), and Ni (2.5 eV), respectively, all lie in the 2.2–3.1 eV range; see Fig. 2. By contrast, the ideal U values (based on oxidation enthalpies) for similar reactions modeled with DFT-GGA span a ~ 3 eV range (i.e., from 3–6 eV [23]). Thus, SCAN incurs consistently similar (qualitatively and quantitatively) SIEs across the 3d series compared to other XC functionals. The quantitative level of SIE within SCAN is also similar for f orbitals, as indicated by a U requirement of 2.0 eV [22] for Ce ($f^1 \rightarrow f^0$). The ideal U value drops as reactions involving higher oxidation states are considered (e.g., V⁴⁺ \rightarrow V⁵⁺, Mn³⁺ \rightarrow Mn⁴⁺, etc.), consistent with the lower number of available (and unpaired) d electrons and consequently lower SIE. Note that the highest U correction (with SCAN+ U) is needed for Fe (3.1 eV), consistent with the highest number of unpaired d electrons exhibited by Fe³⁺ (and hence highest possible SIE). In contrast, U values typically used with GGA (and LDA) [23,33,36] are usually nonmonotonic, with several studies reporting higher U values for Ni systems compared to Fe

[23,33]. This is further verification that SCAN is a more accurate XC functional than GGA or LDA.

Cr oxides with SCAN(+ U) present a significant anomaly since there is no U correction required for reliable thermodynamic, structural, electronic, and magnetic behavior predictions. Intuitively, Cr would require an optimal U similar to V, since Cr oxides exhibit similar numbers of unpaired d electrons compared to V. For example, both Cr₂O₃ and VO have three unpaired d electrons while CrO₂ and V₂O₃ each have two unpaired d electrons. However, the highest ideal U derived from oxidation reactions with Cr (Cr₂O₃ → CrO₂) is 0.5 eV [Fig. 2(c)], significantly lower than the highest ideal U for VO → V₂O₃ [~2.2 eV; Fig. 2(b)]. This anomalous behavior of Cr can be attributed to two specific properties: (i) the metastability of CrO and (ii) the metallic behavior of CrO₂. For $3d$ systems ranging from V to Ni, CrO is the only MO ($M = 3d$) oxide that is metastable. Importantly, Cr should exhibit the highest number of unpaired d electrons (four) in CrO, which might have required a substantial U correction, if CrO had been thermodynamically stable. Instead, DFT-SCAN may benefit from subtle error cancellation due to the inherent metastability of CrO since any experimental measurement on CrO is bound to be error prone; thus errors made by theory fortuitously may compensate errors in experiments. Similarly, CrO₂ is the only MO₂ system ($M = \text{Ti, V, Cr, Mn}$) which is thermodynamically stable and remains metallic at low temperatures [79]. By construction, DFT-SCAN is better suited to describe metallic solids than SCAN+ U , since there is no requirement to impose partial electron localization (by adding U) on Cr's d orbitals. Hence, DFT-SCAN might benefit from the uniqueness of binary Cr oxides, which eventually makes a U correction unnecessary.

Significant challenges still remain in first-principles simulation of $3d$ (and $3d$ -based) oxides. For example, the lack of PAW potentials optimized at the DFT-SCAN level may contribute to significant and unsystematic errors. Specifically, we find that self-consistently optimizing more outer-core electrons with the PAW-PBE potential in Cu significantly worsens the oxidation enthalpy prediction of Cu₂O → CuO (Fig. S2), which may be attributed to the inconsistent use of PAW-PBE projectors with a SCAN XC functional. Cu oxides also represent a unique scenario wherein DFT-SCAN yields the best accuracy for redox thermodynamics whereas SCAN+ U describes the electronic structure more accurately. Notably, we find an error in formation enthalpy of ~0.6 eV/O₂ for ZnO from its pure constituents (Zn and O₂) with DFT-SCAN, similar to the value observed for Cu₂O (from Cu and O₂), where both ZnO and Cu₂O have filled d shells (Table S4). On the other hand, the formation enthalpy of Sc₂O₃ (from Sc and O₂), which has an empty d shell, has an error of <0.1 eV/O₂ with DFT-SCAN (Table S4). Thus, for oxides with a filled d (or f) shell, the use of PAW-PBE potentials with a SCAN XC functional may be problematic. Recently, Bartók and Yates developed the regularized SCAN (rSCAN) functional [118], which removes the numerical instabilities within SCAN and possibly enables building a PAW potential at the DFT-SCAN level. However, more studies are required to ascertain the suitability of the rSCAN (or similar extensions of SCAN) for different systems and to eventually construct SCAN-PAW potentials for all elements.

In the case of Co oxides, the use of U_{Co} with SCAN should be done only if SCAN+ U_{Co} predicts electronic properties in agreement with either experiments or more accurate quantum mechanics calculations. This is illustrated by the example of metastable CoO₂, where SCAN+ U_{Co} 's electronic property prediction can be significantly different from experimental observation. Furthermore, a source of error, particularly in layered compounds (e.g., CoO₂), is the lack of van der Waals corrections with either DFT-SCAN or SCAN+ U . More exploration is required on how the addition of van der Waals corrections affects property prediction by both theoretical frameworks [117].

V. CONCLUSIONS

Useful for a wide range of applications based on their redox activity, $3d$ transition-metal oxides are an important class of materials whose properties must be predicted accurately by any theoretical framework that will be used for materials design and discovery, such as DFT. Notably, the recently developed SCAN XC functional represents an important step forward in improving the overall accuracy of simulations using DFT approximations. However, DFT-SCAN is not immune to SIE [22], particularly when describing the highly correlated d or f electrons, which can be corrected partially by adding an appropriately determined Hubbard U correction. Extending our previous work developing optimal U values (within SCAN+ U) for Fe, Mn, and Ce oxides [22], here we evaluated the optimal U for Ti (2.5 eV), V (1.0 eV), Cr (0.0 eV), Co (3.0 eV), Ni (2.5 eV), and Cu (0.0 eV), using experimental oxidation enthalpies as benchmarks. We found that the added U correction makes significant improvements in predicting redox thermodynamics, ground-state structure, electronic behavior, and magnetic properties in Ti, V, Co, and Ni oxides. For Cr and Cu oxides, we found DFT-SCAN to be more accurate than SCAN+ U for oxidation enthalpy predictions. Further, the transferability of our optimal U values was tested by validating SCAN(+ U) predictions against experimental data for oxides that were not used in obtaining the optimal U . Finally, we identified further work needed to improve the accuracy of DFT-based frameworks in modeling $3d$ oxides.

ACKNOWLEDGMENTS

E.A.C. thanks the US Department of Energy, Office of Energy Efficiency and Renewable Energy, under Award No. DE-EE0008090 for funding this project. O.L. acknowledges financial support from the Princeton Office of Undergraduate Research. The authors thank Princeton Research Computing resources at Princeton University, a consortium of groups including the Princeton Institute for Computational Science and Engineering and the Princeton University Office of Information Technology's Research Computing department. The authors also acknowledge computational resources sponsored by the Department of Energy's Office of Energy Efficiency and Renewable Energy located at the National Renewable Energy Laboratory.

- [1] L. C. Seitz, C. F. Dickens, K. Nishio, Y. Hikita, J. Montoya, A. Doyle, C. Kirk, A. Vojvodic, H. Y. Hwang, J. K. Nørskov, and T. F. Jaramillo, *Science* **353**, 1011 (2016).
- [2] P. Liao and E. A. Carter, *Chem. Soc. Rev.* **42**, 2401 (2013).
- [3] J. Zaffran and M. C. Toroker, *ChemPhysChem* **17**, 1630 (2016).
- [4] T. Ohzuku and A. Ueda, *Solid State Ionics* **69**, 201 (1994).
- [5] M. S. Whittingham, *Chem. Rev.* **114**, 11414 (2014).
- [6] P. Canepa, G. Sai Gautam, D. C. Hannah, R. Malik, M. Liu, K. G. Gallagher, K. A. Persson, and G. Ceder, *Chem. Rev.* **117**, 4287 (2017).
- [7] M. Grätzel, *J. Photochem. Photobiol. C Photochem. Rev.* **4**, 145 (2003).
- [8] V. Shrotriya, G. Li, Y. Yao, C.-W. Chu, and Y. Yang, *Appl. Phys. Lett.* **88**, 073508 (2006).
- [9] G. Sai Gautam, T. P. Senftle, N. Alidoust, and E. A. Carter, *J. Phys. Chem. C* **122**, 27107 (2018).
- [10] G. E. Beghi, *Hydrogen Systems* (Elsevier, Beijing, China, 1986), pp. 153–171.
- [11] C. N. R. Rao and S. Dey, *Proc. Natl. Acad. Sci. USA* **114**, 13385 (2017).
- [12] A. Steinfeld, *Sol. Energy* **78**, 603 (2005).
- [13] N. P. Siegel, J. E. Miller, I. Ermanoski, R. B. Diver, and E. B. Stechel, *Ind. Eng. Chem. Res.* **52**, 3276 (2013).
- [14] P. Hohenberg and W. Kohn, *Phys. Rev.* **136**, B864 (1964).
- [15] W. Kohn and L. J. Sham, *Phys. Rev.* **140**, A1133 (1965).
- [16] J. Sun, A. Ruzsinszky, and J. P. Perdew, *Phys. Rev. Lett.* **115**, 036402 (2015).
- [17] R. Car, *Nat. Chem.* **8**, 820 (2016).
- [18] J. P. Perdew, K. Burke, and M. Ernzerhof, *Phys. Rev. Lett.* **77**, 3865 (1996).
- [19] Y. Zhang, D. A. Kitchaev, J. Yang, T. Chen, S. T. Dacek, R. A. Sarmiento-Pérez, M. A. L. Marques, H. Peng, G. Ceder, J. P. Perdew, and J. Sun, *Npj Comput. Mater.* **4**, 9 (2018).
- [20] D. A. Kitchaev, H. Peng, Y. Liu, J. Sun, J. P. Perdew, and G. Ceder, *Phys. Rev. B* **93**, 045132 (2016).
- [21] J. H. Yang, D. A. Kitchaev, and G. Ceder, *Phys. Rev. B* **100**, 035132 (2019).
- [22] G. Sai Gautam and E. A. Carter, *Phys. Rev. Mater.* **2**, 095401 (2018).
- [23] L. Wang, T. Maxisch, and G. Ceder, *Phys. Rev. B* **73**, 195107 (2006).
- [24] D. C. Patton, D. V. Porezag, and M. R. Pederson, *Phys. Rev. B* **55**, 7454 (1997).
- [25] B. Hammer, L. B. Hansen, and J. K. Nørskov, *Phys. Rev. B* **59**, 7413 (1999).
- [26] J. P. Perdew, *Adv. Quantum Chem.* **21**, 113 (1990).
- [27] J. P. Perdew and A. Zunger, *Phys. Rev. B* **23**, 5048 (1981).
- [28] V. I. Anisimov, J. Zaanen, and O. K. Andersen, *Phys. Rev. B* **44**, 943 (1991).
- [29] M. Cococcioni, *A LDA+U Study of Selected Iron Compounds* (International School for Advanced Studies-SISSA, Trieste, 2002).
- [30] N. J. Mosey and E. A. Carter, *Phys. Rev. B* **76**, 155123 (2007).
- [31] N. J. Mosey, P. Liao, and E. A. Carter, *J. Chem. Phys.* **129**, 014103 (2008).
- [32] M. Cococcioni and S. de Gironcoli, *Phys. Rev. B* **71**, 035105 (2005).
- [33] F. Zhou, M. Cococcioni, C. Marianetti, D. Morgan, and G. Ceder, *Phys. Rev. B* **70**, 235121 (2004).
- [34] I. Timrov, N. Marzari, and M. Cococcioni, *Phys. Rev. B* **98**, 085127 (2018).
- [35] K. Yu and E. A. Carter, *J. Chem. Phys.* **140**, 121105 (2014).
- [36] A. Jain, G. Hautier, S. P. Ong, C. J. Moore, C. C. Fischer, K. A. Persson, and G. Ceder, *Phys. Rev. B* **84**, 045115 (2011).
- [37] S. Lutfalla, V. Shapovalov, and A. T. Bell, *J. Chem. Theory Comput.* **7**, 2218 (2011).
- [38] C. Loschen, J. Carrasco, K. M. Neyman, and F. Illas, *Phys. Rev. B* **75**, 035115 (2007).
- [39] G. Kresse and J. Hafner, *Phys. Rev. B* **47**, 558 (1993).
- [40] G. Kresse and J. Furthmüller, *Phys. Rev. B* **54**, 11169 (1996).
- [41] G. Kresse and D. Joubert, *Phys. Rev. B* **59**, 1758 (1999).
- [42] See Supplemental Material at <http://link.aps.org/supplemental/10.1103/PhysRevMaterials.4.045401> for details on the projector augmented-wave potentials used, crystal structures of all compounds used in transferability checks, effect of including outer core 3p electrons self-consistently in copper oxides, electronic structure of titanium, vanadium, chromium, cobalt, and nickel oxides used in obtaining optimal U values, polymorphs of TiO₂ and antiferromagnetic configurations of zinc blende CoO, calculated on-site magnetic moments in SrCoO₃, transferability checks in nickel and copper oxides, and formation energies of Sc₂O₃ and ZnO calculated using DFT-SCAN.
- [43] H. J. Monkhorst and J. D. Pack, *Phys. Rev. B* **13**, 5188 (1976).
- [44] K.-M. Ho, C. L. Fu, B. N. Harmon, W. Weber, and D. R. Hamann, *Phys. Rev. Lett.* **49**, 673 (1982).
- [45] S. L. Dudarev, G. A. Botton, S. Y. Savrasov, C. J. Humphreys, and A. P. Sutton, *Phys. Rev. B* **57**, 1505 (1998).
- [46] O. Kubaschewski, E. L. Evans, and C. B. Alcock, *Materials Thermochemistry*, 6th ed. (Pergamon Press, Oxford, 1993).
- [47] D. D. Wagman, *The NBS Tables of Chemical Thermodynamic Properties: Selected Values for Inorganic and C₁ and C₂ Organic Substances in SI Units* (American Chemical Society and the American Institute of Physics for the National Bureau of Standards, Washington, DC, 1982).
- [48] I. Barin, *Thermochemical Data of Pure Substances*, 3rd ed. (John Wiley & Sons Ltd., New York, USA 1995).
- [49] M. Hellenbrandt, *Crystallogr. Rev.* **10**, 17 (2004).
- [50] W. L. Roth, *Phys. Rev.* **110**, 1333 (1958).
- [51] W. C. Mackrodt, D. S. Middlemiss, and T. G. Owens, *Phys. Rev. B* **69**, 115119 (2004).
- [52] B. K. Meyer, A. Polity, D. Reppin, M. Becker, P. Hering, P. J. Klar, T. Sander, C. Reindl, J. Benz, M. Eickhoff, C. Heiliger, M. Heinemann, J. Bläsing, A. Krost, S. Shokovets, C. Müller, and C. Ronning, *Phys. Status Solidi* **249**, 1487 (2012).
- [53] M. Heinemann, B. Eifert, and C. Heiliger, *Phys. Rev. B* **87**, 115111 (2013).
- [54] T. Shimizu, T. Matsumoto, A. Goto, T. V. Chandrasekhar Rao, K. Yoshimura, and K. Kosuge, *Phys. Rev. B* **68**, 224433 (2003).
- [55] B. X. Yang, J. M. Tranquada, and G. Shirane, *Phys. Rev. B* **38**, 174 (1988).
- [56] W. L. Roth, *J. Phys. Chem. Solids* **25**, 1 (1964).
- [57] Z. Hu and H. Metiu, *J. Phys. Chem. C* **115**, 5841 (2011).
- [58] Y. Guo, S. J. Clark, and J. Robertson, *J. Phys.: Condens. Matter* **24**, 325504 (2012).
- [59] S. C. Abrahams, *Phys. Rev.* **130**, 2230 (1963).
- [60] P. D. Dernier and M. Marezio, *Phys. Rev. B* **2**, 3771 (1970).
- [61] N. F. Mott and L. Friedman, *Philos. Mag.* **30**, 389 (1974).

- [62] M. Imada, A. Fujimori, and Y. Tokura, *Rev. Mod. Phys.* **70**, 1039 (1998).
- [63] J. S. Stephens and D. W. J. Cruickshank, *Acta Crystallogr., Sect. B: Struct. Crystallogr. Cryst. Chem.* **26**, 222 (1970).
- [64] R. Enjalbert and J. Galy, *Acta Crystallogr., Sect. C* **42**, 1467 (1986).
- [65] E. Povoden, A. N. Grundy, and L. J. Gauckler, *J. Phase Equilibria Diffus.* **27**, 353 (2006).
- [66] M. Pavone, A. M. Ritzmann, and E. A. Carter, *Energy Environ. Sci.* **4**, 4933 (2011).
- [67] N. Alidoust, M. Lessio, and E. A. Carter, *J. Appl. Phys.* **119**, 025102 (2016).
- [68] N. Charles and J. M. Rondinelli, *Phys. Rev. B* **94**, 174108 (2016).
- [69] M. Uchida, J. Fujioka, Y. Onose, and Y. Tokura, *Phys. Rev. Lett.* **101**, 066406 (2008).
- [70] R. M. Moon, T. Riste, W. C. Koehler, and S. C. Abrahams, *J. Appl. Phys.* **40**, 1445 (1969).
- [71] N. Serpone, *J. Phys. Chem. B* **110**, 24287 (2006).
- [72] S. Shin, S. Suga, M. Taniguchi, M. Fujisawa, H. Kanzaki, A. Fujimori, H. Daimon, Y. Ueda, K. Kosuge, and S. Kachi, *Phys. Rev. B* **41**, 4993 (1990).
- [73] R. M. Moon, *Phys. Rev. Lett.* **25**, 527 (1970).
- [74] S. Shin, Y. Tezuka, T. Kinoshita, A. Kakizaki, T. Ishii, Y. Ueda, W. Jang, H. Takei, Y. Chiba, and M. Ishigame, *Phys. Rev. B* **46**, 9224 (1992).
- [75] P. Leroux-Hugon and D. Paquet, *J. Phys. Colloq.* **41**, C5 (1980).
- [76] A. Kumar, P. Singh, N. Kulkarni, and D. Kaur, *Thin Solid Films* **516**, 912 (2008).
- [77] M. M. Abdullah, F. M. Rajab, and S. M. Al-Abbas, *AIP Adv.* **4**, 027121 (2014).
- [78] L. M. Corliss, J. M. Hastings, R. Nathans, and G. Shirane, *J. Appl. Phys.* **36**, 1099 (1965).
- [79] J. M. D. Coey and M. Venkatesan, *J. Appl. Phys.* **91**, 8345 (2002).
- [80] R. H. Misho, W. A. Murad, and G. H. Fattahallah, *Thin Solid Films* **169**, 235 (1989).
- [81] J. van Elp, J. L. Wieland, H. Eskes, P. Kuiper, G. A. Sawatzky, F. M. F. de Groot, and T. S. Turner, *Phys. Rev. B* **44**, 6090 (1991).
- [82] P. Wei and Z. Q. Qi, *Phys. Rev. B* **49**, 10864 (1994).
- [83] D. C. Khan and R. A. Erickson, *Phys. Rev. B* **1**, 2243 (1970).
- [84] G. A. Sawatzky and J. W. Allen, *Phys. Rev. Lett.* **53**, 2339 (1984).
- [85] A. K. Cheetham and D. A. O. Hope, *Phys. Rev. B* **27**, 6964 (1983).
- [86] F. Reynaud, A. M. Ghorayeb, Y. Ksari, N. Menguy, A. Stepanov, and C. Delmas, *Eur. Phys. J. B* **14**, 83 (2000).
- [87] F. Reynaud, D. Mertz, F. Celestini, J.-M. Debierre, A. M. Ghorayeb, P. Simon, A. Stepanov, J. Voiron, and C. Delmas, *Phys. Rev. Lett.* **86**, 3638 (2001).
- [88] L. Zhang, L. McMillon, and J. McNatt, *Sol. Energy Mater. Sol. Cells* **108**, 230 (2013).
- [89] J. Ghijsen, L. H. Tjeng, J. van Elp, H. Eskes, J. Westerink, G. A. Sawatzky, and M. T. Czyzyk, *Phys. Rev. B* **38**, 11322 (1988).
- [90] G. Sai Gautam, T. P. Senftle, and E. A. Carter, *Chem. Mater.* **30**, 4543 (2018).
- [91] K. Yu and E. A. Carter, *Chem. Mater.* **28**, 864 (2016).
- [92] M. K. Aydinol, A. F. Kohan, and G. Ceder, *J. Power Sources* **68**, 664 (1997).
- [93] J. C. Slater, *Phys. Rev.* **36**, 57 (1930).
- [94] J. P. Perdew, W. Yang, K. Burke, Z. Yang, E. K. U. Gross, M. Scheffler, G. E. Scuseria, T. M. Henderson, I. Y. Zhang, A. Ruzsinszky, H. Peng, J. Sun, E. Trushin, and A. Görling, *Proc. Natl. Acad. Sci. USA* **114**, 2801 (2017).
- [95] D. A. H. Hanaor and C. C. Sorrell, *J. Mater. Sci.* **46**, 855 (2011).
- [96] Y. Luo, A. Benali, L. Shulenburger, J. T. Krogel, O. Heinonen, and P. R. C. Kent, *New J. Phys.* **18**, 113049 (2016).
- [97] J. Trail, B. Monserrat, P. López Ríos, R. Maezono, and R. J. Needs, *Phys. Rev. B* **95**, 121108 (2017).
- [98] M. E. Arroyo-de Dompablo, A. Morales-García, and M. Taravillo, *J. Chem. Phys.* **135**, 054503 (2011).
- [99] M. T. Curnan and J. R. Kitchin, *J. Phys. Chem. C* **119**, 21060 (2015).
- [100] M. Landmann, E. Rauls, and W. G. Schmidt, *J. Phys.: Condens. Matter* **24**, 195503 (2012).
- [101] E. Finazzi, C. Di Valentin, G. Pacchioni, and A. Selloni, *J. Chem. Phys.* **129**, 154113 (2008).
- [102] R. Zimmermann, P. Steiner, R. Claessen, F. Reinert, S. Hüfner, P. Blaha, and P. Dufek, *J. Phys.: Condens. Matter* **11**, 1657 (1999).
- [103] M. J. Redman and E. G. Steward, *Nature (London)* **193**, 867 (1962).
- [104] N.-N. Sun and H.-Y. Wang, *J. Magn. Magn. Mater.* **454**, 176 (2018).
- [105] D.-H. Seo, A. Urban, and G. Ceder, *Phys. Rev. B* **92**, 115118 (2015).
- [106] M. Reehuis, M. Tovar, D. M. Többens, P. Pattison, A. Hoser, and B. Lake, *Phys. Rev. B* **91**, 024407 (2015).
- [107] M. Enhessari, A. Salehabadi, S. Khanahmadzadeh, K. Arkat, and J. Nouri, *High Temp. Mater. Processes* **36**, 121 (2017).
- [108] M.-H. Whangbo and H.-J. Koo, *Inorg. Chem.* **41**, 3570 (2002).
- [109] J. F. Pierson, A. Thobor-Keck, and A. Billard, *Appl. Surf. Sci.* **210**, 359 (2003).
- [110] M. Onoda, *J. Solid State Chem.* **136**, 67 (1998).
- [111] C. H. Lin, S. Y. Chen, and P. Shen, *J. Phys. Chem. C* **113**, 16356 (2009).
- [112] Y. Long, Y. Kaneko, S. Ishiwata, Y. Taguchi, and Y. Tokura, *J. Phys.: Condens. Matter* **23**, 245601 (2011).
- [113] C. Delmas, C. Fouassier, and P. Hagemuller, *Phys. B+C* **99**, 81 (1980).
- [114] G. G. Amatucci, J. M. Tarascon, and L. C. Klein, *J. Electrochem. Soc.* **143**, 1114 (1996).
- [115] T. Motohashi, T. Ono, Y. Sugimoto, Y. Masubuchi, S. Kikkawa, R. Kanno, M. Karppinen, and H. Yamauchi, *Phys. Rev. B* **80**, 165114 (2009).
- [116] H. Peng, Z.-H. Yang, J. P. Perdew, and J. Sun, *Phys. Rev. X* **6**, 041005 (2016).
- [117] F. Tran, L. Kalantari, B. Traoré, X. Rocquefelte, and P. Blaha, *Phys. Rev. Mater.* **3**, 063602 (2019).
- [118] A. P. Bartók and J. R. Yates, *J. Chem. Phys.* **150**, 161101 (2019).